A canonical framework for modeling elasto-viscoplasticity in complex fluids

Citation: Dimitriou, Christopher J. and Gareth H. McKinley. "A canonical framework for modeling elasto-viscoplasticity in complex fluids" Journal of Non-Newtonian Fluid Mechanics 265 (March 2019): 116-132. © 2018 Elsevier B.V.

As Published: 10.1016/J.JNNFM.2018.10.004

Publisher: Elsevier BV

Persistent URL: https://hdl.handle.net/1721.1/129784

Version: Original manuscript: author's manuscript prior to formal peer review

A Canonical Framework for Modeling Elasto-Viscoplasticity in Complex Fluids

Christopher J. Dimitriou, Gareth H. McKinley

77 Massachusetts Avenue, Cambridge, MA 02139

Abstract

A comprehensive framework for modeling elasto-viscoplasticity in complex fluids is discussed. It is based on the plasticity mechanism of kinematic hardening, which is widely accepted in solid mechanics and accounts for transient yielding processes. We discuss a simple one dimensional variant of the model, as well as a fully three-dimensional, frame-invariant and thermodynamically admissible version of the model. Predictions for several canonical rheometric test protocols are provided. We also discuss possible extensions to account for additional rheological complexities exhibited by real fluids, such as thixotropy, nonlinear elasticity and normal stress differences. We find that this framework has several advantages over the more commonly used elastic Bingham-like or elastic Herschel Bulkley models for describing elasto-viscoplasticity. First, the model can account for behavior over a much wider range of viscometric test conditions. Second, it eliminates the flow/no flow criterion inherent in Bingham-like constitutive laws, which frequently requires regularization. Third, it is a flexible framework and allows for implementation of additional complexities, including thixotropic behavior and other nonlinear rheological features.

Keywords: Yield-Stress Fluids, Viscoplasticity, Constitutive modeling

1. Introduction

Elasto-Viscoplastic (or EVP) behavior is frequently exhibited by a range of complex fluids, including many foods, consumer products and industrial materials [1]. EVP behavior is generally characterized by a yield-like transition that occurs when the stress imposed on a soft solid exceeds a critical value. Below this stress, the material behaves primarily as

an elastic solid, whereas above the critical stress the material flows like a liquid. Complex fluids that exhibit EVP behavior are often called "yield stress fluids", and a wide range of fluids are known to exhibit this behavior [2, 1].

Most constitutive models that are used to describe viscoplastic behavior are based on the well-known Bingham or Herschel-Bulkley models. These two models assume the following relation between the magnitude of the stress $|\sigma|$ and the magnitude of the strain rate $|\dot{\gamma}|$,

$$|\sigma| = \sigma_y + k|\dot{\gamma}|^m \ , \tag{1}$$

where σ_y is the critical yield stress, k is a viscosity coefficient (with units Pa.s^m), and m is a power law exponent. For the case of $m = 1$, the constitutive model above reduces to the simplest model for yield stress fluids, the Bingham model, with $k \to \mu_p$ being the plastic viscosity.

Oldroyd [3] was the first to propose a frame-invariant, three-dimensional generalization of the Bingham model. This Oldroyd-Bingham model (we borrow this term from Goddard [4]) for EVP materials specifies the following relationship between the Cauchy stress $\mathbf{T}$ and the rate of deformation tensor $\mathbf{D}$

$$\mathbf{T}_0 = 2G\mathbf{E} \qquad \text{If } |\mathbf{T}_0| < \sqrt{2}\sigma_y \tag{2}$$

$$\mathbf{T}_0 = 2k\mathbf{D} + \sqrt{2}\sigma_y \frac{\mathbf{D}}{|\mathbf{D}|} \qquad \text{If } |\mathbf{T}_0| \geq \sqrt{2}\sigma_y \tag{3}$$

In the above equations, $\mathbf{T}_0$ is the deviatoric Cauchy stress defined as $\mathbf{T}_0 \equiv \mathbf{T} - \frac{1}{3}\text{tr}(\mathbf{T})$. The tensor $\mathbf{E}$ is the infinitesimal strain tensor defined as $\mathbf{E} \equiv \frac{1}{2}(\mathbf{H} + \mathbf{H}^\intercal)$, where $\mathbf{H}$ is the displacement gradient, defined as $\mathbf{H} \equiv \nabla\mathbf{u}$. The vector $\mathbf{u}$ is the displacement of material points from an undeformed reference configuration $\mathbf{X}$, and is given by $\mathbf{u} = \mathbf{x} - \mathbf{X}$. The vector $\mathbf{x}$ describes the spatial location of the material points $\mathbf{X}$ after a deformation. With the notation adopted herein,[1] the components of the displacement gradient $\mathbf{H}$ are given by

[1] Throughout this manuscript we adopt the notation employed in [5] to describe various tensorial constitutive models. However we include footnotes in certain instances where it is necessary to clarify the differences between the continuum mechanics notation employed in [5], and the notation typically employed in the rheology literature, such as in [6] and [7].

$H_{ij} = \frac{\partial u_i}{\partial X_j}$, where u_i are the cartesian components of the displacement vector $\mathbf{u}$, and X_j are the cartesian components of the material reference points $\mathbf{X}$.

The rate of deformation tensor is defined as $\mathbf{D} \equiv \frac{1}{2}(\mathbf{L} + \mathbf{L}^\intercal)$, where $\mathbf{L}$ is the velocity gradient defined as $\mathbf{L} \equiv \text{grad}\,\mathbf{v}$. The components of $\mathbf{L}$ are given by $L_{ij} = \frac{\partial v_i}{\partial x_j}$,[2] where v_i are the cartesian components of the velocity vector $\mathbf{v}$, and x_j are the cartesian components of the spatial points $\mathbf{x}$.[3] In many applications, the elastic shear modulus of the material is assumed to be infinite, so that for $\mathbf{T}_0 \leq \sqrt{2}\sigma_y$ the material is perfectly rigid and there is no deformation, with $\mathbf{E} = 0$ and $\mathbf{D} = 0$.

The above Oldroyd-Bingham model is analogous to other frame-invariant, tensorial constitutive models used for viscoelastic fluids (e.g. the Upper-Convected Maxwell model or Oldroyd-B model). It can be used for numerical simulations of more complex flow scenarios, which necessarily require a model of tensorial form. There are therefore a large number of contributions to the literature in which versions of this model have served as a basis for understanding complex flows of viscoplastic liquids [8, 9, 10, 11, 12, 13, 14, 15]. From that perspective, it serves as the current canonical framework for modeling viscoplasticity in complex fluids.

Despite its widespread use, the Oldroyd-Bingham model is extremely simplified, and has several known deficiencies that prevent it from fully describing the response of real materials. One drawback of the model form given in Eqs 2-3 is that it gives unphysical predictions for transient viscometric responses during startup of steady flow or oscillatory flow [16, 17]. For example, when a constant deformation rate $\mathbf{D}$ is applied on the material, there is an initial elastic deformation with the stress $\mathbf{T}_0$ increasing linearly with the imposed strain.

[2] The tensor $\mathbf{L}$ used here (and in [5]) is the same as the tensor $(\nabla\mathbf{v})^\dagger$ in [6]

[3] Based on the approach followed in [5], we make a distinction between the grad and ∇ operator for taking gradients of vectors. The different operators are utilized to distinguish between "spatial gradients" and "material gradients". Hence $\nabla \equiv \frac{\partial}{\partial \mathbf{X}}$ is a gradient with respect to some "material" undeformed reference configuration, and grad $\equiv \frac{\partial}{\partial \mathbf{x}}$ is a gradient with respect to some "spatial" deformed configuration of the body. From Eq. 9.2 in [5] and Eq. 9.2-9 in [6], $\nabla\mathbf{v} = (\text{grad}\mathbf{v})\mathbf{F}$, where $\mathbf{F}$ is the deformation gradient tensor. Note that the original Oldroyd model described in [3] appears to use the grad operator to define both $\mathbf{E}$ and $\mathbf{D}$ (or ϵ_{ij} and e_{ij} respectively, using the notation in [3])

When the material reaches the yield point, the stress then exhibits a jump discontinuity due to the presence of the rate-dependent term $2k\mathbf{D}$ in Eq. 3. These discontinuities can be avoided by decomposing the material deformation into separate elastic and plastic parts, which is a commonly taken approach to model plasticity. More recent models, such as those used Marmottant and Graner [18], Benito et al. [19] and Saramito [20, 21] have taken this approach.

Another drawback of the Oldroyd-Bingham framework is that it only predicts linear elastic behavior when the stress in the material is below the critical stress or yield stress σ_y. Many real yield stress fluids such as soft gels do not behave in this manner. Their behavior is usually elastically-dominated pre-yield, but some important aspects of viscous or dissipative behavior are still present. For example, most yield stress fluids will exhibit a finite (albeit small) value of the loss modulus $G''(\omega)$ over a wide range of oscillatory frequencies, indicating that the material experiences dissipative losses and some irreversible deformation below the yield stress. For example, Carbopol microgels, which are a commonly-studied ideal yield stress fluid [22], exhibit transient elastoplastic creeping flow below their yield stress [23, 24]. This type of behavior is ubiquitous among yield stress fluids [2], and the Oldroyd-Bingham framework cannot account for it.

An important issue pertaining to numerical simulations of the Oldroyd-Bingham model is the determination of the correct regularization protocol of the equations given in Eq. 3-2 [25, 15, 26]. The discontinuous nature of the equations for Bingham-like models require solving for the *a priori* unknown spatial location of a yield surface, across which the material changes from its yielded to its unyielded state [25, 15, 26, 27]; this can be computationally expensive. To avoid these numerical issues, the form of the equations given in Eqs. 3-2 can be regularized by specifying a very large but finite zero shear rate viscosity at low values of $|\mathbf{D}|$. The Papanastasiou model is one frequently used regularization scheme [28]. With the specification of a large zero shear rate viscosity, the model then predicts a very slow, but non-zero, creeping flow which will occur at all stresses below the yield stress σ_y. However, this is only a first order approximation of the behavior of real materials. Measurements in real yield stress fluids show a time-varying apparent viscosity at low stresses below the yield

stress [24]. Creeping flow below the yield stress is therefore a transient phenomenon, and not a steady state one which can be characterized by a single viscosity parameter [29] .

In a recent publication, Dimitriou et al. introduced a model based on the plasticity mechanism of kinematic hardening (KH) to capture the response of an "ideal" yield stress fluid to a wide variety of rheological deformation histories [30]. Among the test protocols considered were large amplitude oscillatory shear (LAOS) tests, which have proven difficult to predict accurately with a simple constitutive law, due to their inherently nonlinear and time-varying nature as the stress amplitude periodically varies across the yield envelope of the material. The "KH model" that was introduced in [30] and [31] showed several quantitative improvements over a simpler elastic-Herschel-Bulkley model for describing Carbopol gels undergoing transient deformation histories. The goal of the present work is to provide a thorough discussion of the rheological predictions of this KH model and its extensions, thereby elucidating the benefits that it can provide as a future canonical framework for use in numerical simulations or theoretical applications.

We first discuss a simple, one-dimensional version of the model and derive analytical expressions for the model predictions in steady shear, creep and small amplitude oscillatory shear. Then we formulate a fully frame-invariant, thermodynamically admissible, three-dimensional version of the model. We will discuss how to convert the model from its natural Lagrangian framework to an Eulerian framework, which is more appropriate for numerical simulations of steady flow scenarios. Model predictions for several different common rheometric flow histories (shear, extension) are provided, and we identify the similarities between this model and other tensorial constitutive models for complex fluids.

As a canonical framework, this KH model possesses several improvements over the Oldroyd-Bingham framework. It is able to predict the slow irreversible transient creeping deformation that many yield-stress fluids exhibit. It has also been successful at predicting experimental data of EVP materials under large amplitude oscillatory shear [30, 31]. Furthermore, it eliminates the stress discontinuity and conditional statement required for identifying if/when yielding behavior is present in a material. Finally, it is a flexible framework, and allows for other features of a real material's response to be implemented (e.g.

nonlinear elasticity, or even thixotropy [4, 32]).

2. Results and Discussion

We discuss two different formulations of the KH model. This model was introduced in previous work [30], and was successful at predicting the response of a Carbopol microgel to a number of different steady and oscillatory shearing protocols. We reproduce the model formulation here in two parts: First, a simplified one-dimensional version of the model is introduced. We then show how it can be extended to a generalized three-dimensional, frame-invariant, thermodynamically admissible version of the KH model, which is also provided in the appendix of Dimitriou et al. [30].

2.1. 1D formulation of model

A fundamental mathematical assumption that is used for the KH model is the decomposition of the deformation within the material into two components - an elastic contribution and a plastic contribution. In the case of the three-dimensional version of the KH model, the material's deformation gradient $\mathbf{F}$ is multiplicatively decomposed into plastic and elastic parts using the Kroner decomposition (see Sec. 2.2 for additional details). For the simpler 1D (shear) version of the KH model however, we additively decompose the total shear strain γ as

$$\gamma = \gamma^e + \gamma^p \ , \tag{4}$$

where γ^e is the elastic, reversible part of the shear strain, and γ^p is the irreversible plastic part of the shear strain. The elastic strain is related linearly to the shear stress σ through a shear modulus G

$$\gamma^e = \frac{\sigma}{G} \ . \tag{5}$$

The magnitude of the rate of change of the plastic strain, $|\dot{\gamma}^p|$, is given by a power law "flow rule" of the form

$$|\dot{\gamma}^p| = \left(\frac{|\sigma - \sigma_{\text{back}}|}{k} \right)^{(1/m)} \ , \tag{6}$$

where σ_{back} is a quantity known as the back stress in the material (discussed in further detail below), k is the material consistency, and m is a power law exponent. The stress difference $\sigma - \sigma_{\text{back}}$ is also termed the *effective stress* which is responsible for driving the plastic flow in the material. The direction of plastic strain, n^p, must also be specified:

$$n^p = \frac{\sigma - \sigma_{\text{back}}}{|\sigma - \sigma_{\text{back}}|} \ . \tag{7}$$

The rate of change of plastic strain is then given as the product of its direction and magnitude, i.e. $\dot{\gamma}^p = n^p|\dot{\gamma}^p|$. The plastic strain rate is therefore assumed to be *co-directional* with the effective stress in the material.

A critical component of the KH framework is its ability to account for evolution in the value of the back stress, σ_{back}, as a function of flow history. The back stress represents the center of the yield surface of the material in stress space. It can be related to an internal strain-like variable A, through a back stress modulus C,

$$\sigma_{\text{back}} = CA \ . \tag{8}$$

This internal or "hidden" variable A can be related to variations in the defect energy within the deforming material; this will be discussed further in the following section. For the specific model discussed in this section, the variable A evolves according to the Armstrong-Frederick [33] kinematic hardening equation,

$$\dot{A} = \dot{\gamma}^p - qA|\dot{\gamma}^p| \ , \tag{9}$$

where q is a dimensionless constitutive parameter which governs the change of the material structure due to shearing. As we show below, $1/q$ is also a measure of the yield strain of the material. In what follows we discuss the predictions of the KH model under several different types of simple one-dimensional flows.

Steady simple shear. Under steady shearing conditions, i.e. a nonzero constant value of $\dot{\gamma}^p$, with $\dot{A} = 0$, the KH model given by Eqs. 6-9 reduces to the canonical Herschel-Bulkley relationship between the magnitude of the stress and the shear rate,

$$|\sigma| = C/q + k|\dot{\gamma}^p|^m \ , \tag{10}$$

where the ratio of the KH model parameters $C/q = \sigma_y$ is the steady state yield stress in the material. For almost all actual yield stress materials we expect $m < 1$. While the Herschel-Bulkley model only defines the stress for a nonzero shear rate, in what follows we show how the KH model can provide predictions for deformations occurring at stresses below the critical yield stress C/q.

Creep. For applied stresses below the steady state yield stress, $\sigma_0 < \sigma_y$, the KH model predicts a slow transient creeping flow. Under this creeping deformation, it can be shown (derivation provided in the appendix) that the instantaneous value of the apparent viscosity defined as $\eta^+(t) \equiv \frac{\sigma_0}{\dot{\gamma}^p(t)}$ is given by the following expression

$$\eta^+ \simeq \eta_c \left(\frac{t}{t_c}\right)^{1/(1-m)}, \tag{11}$$

where t_c is a characteristic time scale and η_c is a characteristic viscosity scale. These scales are found to be:

$$t_c \equiv \left(\frac{k}{C}\right)^{1/m}, \tag{12}$$

$$\eta_c \equiv \sigma_0 \left(\frac{k}{C}\right)^{1/m} \left[\left(1 - \frac{q\sigma_0}{C}\right)\left(\frac{1-m}{m}\right)\right]^{1/(1-m)}. \tag{13}$$

The expression in Eq. 11 holds for all values of $m < 1$ (and in the singular limit when $m = 1$, it can be shown that η^+ grows exponentially [34]). The power law growth of the apparent viscosity over time during creep has been observed previously in EVP materials [23]. For carbopol microgels, several authors have measured the exponent which characterizes the growth of viscosity over time. A range of values for this exponent have been experimentally observed across several different carbopol formulations [30, 23, 24, 35, 29]. One subtle aspect of the KH model's predicted creep behavior is that for values of $m < 1$, the quantity $1/(1-m)$ is greater than 1, resulting in the plastic strain in the material increasing for all times, but approaching an asymptotic upper limit. This behavior follows from Eq. 11. With $\dot{\gamma}^p \sim t^{1/(m-1)}$, and $m < 1$, the integral of the plastic strain rate in the limit of $t \to \infty$ converges, so the plastic strain approaches a finite value at long times. Thus, the model does not predict an unbounded power law growth in the total material strain over time.

Some recent experimental work indicates that the strain can grow in an unbounded fashion, at least for one particular carbopol formulation, and within a range of moderate stresses which are below the yield stress [35]. However this behavior appears to vary from material to material, and is not a ubiquitous feature observed across all EVP materials. In the work by Møller et al. [24], some EVP materials exhibited sufficiently fast viscosity growth for the strain to approach an asymptotic limit.

Small amplitude oscillatory shear (SAOS). For the special case where $m = 1$, analytical expressions for $G'(\omega)$ and $G''(\omega)$ for the KH model under small amplitude oscillatory stress ($\sigma = \sigma_0 \cos \omega t$) can be found (see appendix for derivation):

$$\frac{G'(\omega)}{G} = \frac{(1 + G/C) + (k\omega/C)^2}{(1 + G/C)^2 + (k\omega/C)^2} \ , \tag{14}$$

$$\frac{G''(\omega)}{G} = \frac{(G/C)(k\omega/C)}{(1 + G/C)^2 + (k\omega/C)^2} \ . \tag{15}$$

The expressions for $G'(\omega)$ and $G''(\omega)$ above are the same as those for a standard 3-parameter viscoelastic model, with a spring of modulus G in series with a Kelvin element. The Kelvin element consists of a spring with modulus C and a dashpot with viscosity coefficient k, corresponding to a retardation time $\lambda_2 = k/C$.

For the case where $m < 1$, the intrinsically nonlinear form of the plastic flow rule in Eq. 6 results in very strict constraints on the limits of linearity in the imposed deformation. The expressions for the linear viscoelastic moduli reduce to:

$$G'(\omega) = G, \tag{16}$$

$$G''(\omega) = 0 \ . \tag{17}$$

While the expressions above indicate that in the limit of *very* small strains the KH model predicts zero energy dissipation, we will show in the next section that for practical values of the material coefficients, small but finite values of G'' are predicted at small strains (order of 1%) because of additional small but non-negligible contributions from the inherently nonlinear nature of the Armstrong-Frederick kinematic hardening expression in Eq. 9. However, these values asymptotically tend to zero as the strain amplitude approaches zero. It is also

possible to modify the form of the viscoelastic model below the yielding point, in order to accurately capture the experimentally observed frequency-dependent variations on the linear viscoelastic behavior; this has been demonstrated previously in [31]. Although not discussed in detail here, Section 2.4.1 shows various mechanical analogs for simplified versions of the KH model.

LAOS and other transient experiments. Predictions of the model for LAOS (large amplitude oscillatory shear) experiments are discussed in detail in our previous articles [30, 31]. For completeness we briefly review the results from these experiments, because they were the original basis for introducing the mechanism of kinematic hardening to model EVP behavior of yield stress fluids. Specifically, the kinematic hardening mechanism captures the "Bauschinger effect" [36], which is made apparent when data from LAOS experiments are plotted in cyclic stress-strain (Lissajous) curves. The Bauschinger effect results in a distinctive rhomboidal shape of the stress-strain curves [31]. To predict this behavior, a constitutive model must predict a reduction of the yield stress in a direction opposite to the direction the material is being deformed in. For example, when the material is being deformed under shear in a given direction, reversal of the deformation will cause the material to yield at a lower stress in the opposite direction. This requires an understanding of the yield stress as a *directional quantity*, even in the case where the model is used to predict one-dimensional deformations. It is for this reason that the back stress can have either positive or negative values.

The specific form of the kinematic hardening equation which is used here to predict this behavior (Eq. 9) is taken from Armstrong and Frederick [33]. This form is used widely in the plasticity literature, however to our knowledge, prior to [30] it had not been previously utilized to predict yielding behavior in complex fluids. One additional benefit of the Armstrong-Frederick form is the ability of the model to predict transient plastic deformation below the steady state yield stress. Other more sophisticated EVP models can also predict this type of transient plastic deformation, however slow creeping flow will not necessarily result in the correct shape of the predicted Lissajous curves under LAOS (see for example

the LAOS predictions of the Saramito model in [20], which differ distinctly from the model predictions and experimental observations shown in [30] and [31]). Additional extensions to this framework to incorporate multiple relaxation modes have recently been considered by Wei et al. [37].

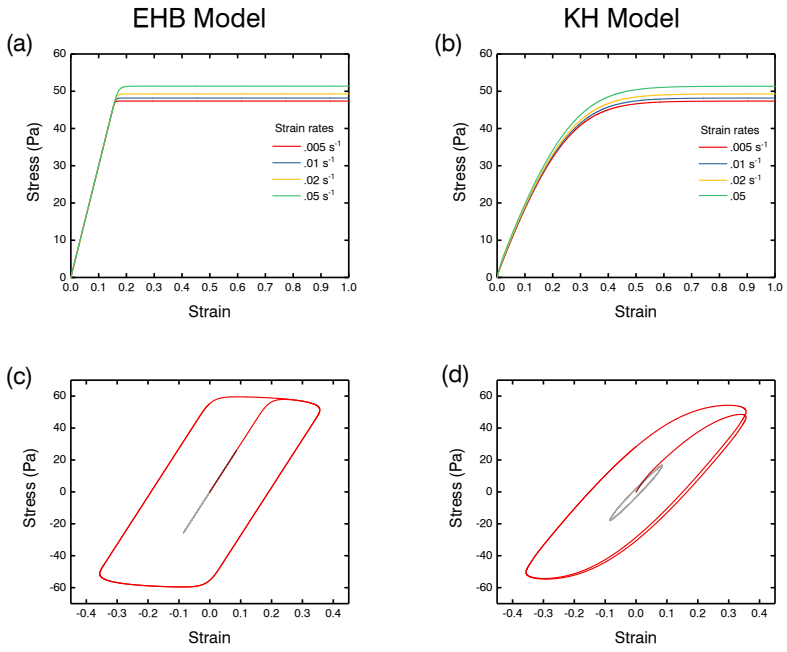

Figure 1: Simulated predictions for the 1D versions of the EHB model and the KH model for startup of steady shear flow ((a) and (b)), and large amplitude oscillatory shear ((c) and (d)). Steady shear startup simulations are carried out at a range of shear rates, while LAOS simulations are carried out at $\gamma_0 = 0.1$ (inner curves) and $\gamma_0 = 0.4$ (outer curves). Values of the model parameters used in these simulations are similar to those used in [30] to model a Carbopol microgel under LAOS: $G = 300$ Pa, $\sigma_y = C/q = 45$ Pa, $C = 540$ Pa, $q = 12$, $k = 23$ Pa.s^m, $m = 0.43$.

The changes that arise due to implementation of the KH mechanism in the generic behavior predicted by EVP models for transient rheological flows is shown in Fig. 1. Model predictions are given for startup of steady shear flow, in addition to large amplitude oscillatory shear. As can be seen in the comparison of Fig. 1 (c) and (d), the introduction of kinematic hardening results in a more gradual transition of the material behavior from a linear elastic solid below yield, to viscoplastic flow above yield. The KH mechanism also

predicts energy dissipation and a continuous frequency and strain dependent evolution of the loss modulus $G''(\omega, \gamma_0)$ as the material deformation approaches the yield point. As discussed by Fraggedakis et al. [38] LAOS can be used as a key test to elucidate this dissipative behavior. In Fig. 1 (d) this is manifested by the nonzero area enclosed within the Lissajous curves plotted for $\gamma_0 = 0.1$. This is contrary to the predictions of the EHB model, where behavior at these strain levels is purely elastic. The comparison of Fig. 1 (a) and (b) (startup of steady shear) further illustrate how implementation of the KH mechanism results in a more gradual (and physically more realistic [30, 39]) transition from an un-yielded to a yielded state in the material. Capturing the correct material response across a range of strains under reversing flows is a key ingredient to correctly predicting the kinematics in complex flows (e.g. sedimentation of a sphere) that involve EVP materials [40, 38].

Summary. The KH framework provides considerable versatility, and offers numerous improvements over the simpler Herschel-Bulkley model. Among these are the ability of the KH model to predict the slow viscoplastic creeping flow (with a power law growth in apparent viscosity) for stresses below the yield stress, $\sigma < \sigma_y$. Real EVP materials are typically observed to exhibit this power-law creeping behavior [23, 24, 30]. The KH model can also accurately predict the response of EVP materials under large amplitude oscillatory shear (LAOS) [30]. The simpler elastic-Bingham model cannot capture these rheological features of EVP materials.

2.1.1. Fitting of KH model to experimental data for a real yield stress fluid

Rheological measurements were carried out on a Carbopol microgel (a minimally thixotropic, "ideal" yield stress fluid [23]) to fit the KH model parameters, as well as to demonstrate the model's versatility in predicting rheological behavior. The two tests that are selected are (1) measurement of the material's steady shearing flowcurve, and (2) measurement of the viscoelastic moduli G' and G'' as a function of strain amplitude γ_0.

The particular Carbopol microgel that is used is a 0.5% wt. 901 variant (manufactured by Lubrizol). Measurements are made with a TA instruments AR-G2 stress-controlled rheometer, with a roughened cone-plate geometry fixture in order to suppress wall slip. The mea-

surement of the steady shearing flowcurve is carried out by imposing a constant shear rate on the material $\dot{\gamma}_0$, and waiting for 3 minutes for the stress to equilibrate. After equilibration, the imposed rate is then increased. For the oscillatory shear measurements of the storage and loss moduli $G'(\omega, \gamma_0)$ and $G''(\omega, \gamma_0)$, tests are carried out at a constant frequency of $\omega = 2$ rad/s and the strain amplitude was steadily increased.

The experimental data, together with a best fit for each data set to the KH model, are given in Fig. 2. The best fit curves are given by solid lines in each of the graphs. As we have shown in Eq 10, The KH model predicts a steady flowcurve identical to the Herschel-Bulkley relation, which has been shown by a number of previous workers to agree well with the measured flowcurves for Carbopol microgels [41]. The measurements of $G'(\gamma_0)$ and $G''(\gamma_0)$ in Fig. 2 (b) show a general trend that is ubiquitous among yield stress fluids. For small values of γ_0, the material exhibits a linear viscoelastic behavior that is dominated by elasticity, with $G' \gg G''$. As the imposed strain amplitude is steadily increased towards the point of yielding, the material response will no longer be linearly viscoelastic. This coincides with a sharp monotonic decrease in the elastic modulus G' as well as an increase in the loss modulus G''. These changes are indicative of a yielding transition in the material, where the behavior changes from solid-like to liquid-like. The loss modulus G'' eventually reaches a maximum, roughly at the point where G' and G'' cross over. The two moduli both then decrease monotonically with γ_0 and G'' continues to exceed G' as the strain amplitude is continuously increased.

The simulated best fit response of the KH model, given by the solid lines in Fig. 2 (b), correctly predicts the changes in $G'(\gamma_0)$ and $G''(\gamma_0)$ of the Carbopol microgel as the strain amplitude is increased. A similar level of "goodness of fit" was also demonstrated by Fraggedakis et al. [40, 38] using the mechanism of kinematic hardening. As has been reported previously [42], the local maximum in G'' at intermediate strains coincides with the crossover point of G' and G'', which the KH model is also able to capture. Furthermore, the KH model predicts a non-zero value of the loss modulus G'' for small but non-zero strain amplitudes, and this value is significantly less than G' (with $\tan\delta \sim 0.2$). Finite values of G'' are present at strain amplitudes on the order of 1%, even though the loss modulus G'' can

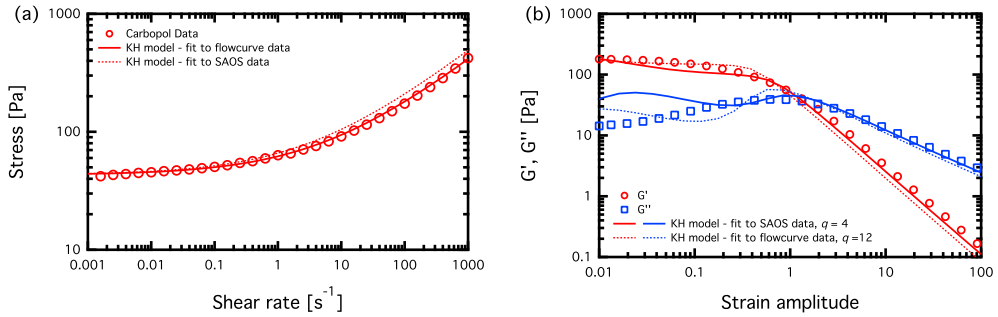

Figure 2: Fit of the KH model discussed in Sec. 2.1 to rheological data for a Carbopol microgel. The flowcurve (i.e. a plot of $|\sigma|$ vs. $|\dot{\gamma}|$) is given in (a), and in (b) the dependency of the storage and loss moduli G' and G'' on strain amplitude γ_0 is plotted. Solid lines are best fits, while dashed lines are fits using model parameters determined from the other data set.

be shown to rigorously approach zero if the abscissa was extended to much smaller values of γ_0. This is in contrast to the elastic-Bingham model, which predicts a constant value of $G' = G$, and an identically zero value of the loss modulus for all strain amplitudes below the yielding point. The only disagreement between the KH model and the experimental data occurs at low strain amplitudes, where the KH model overpredicts the experimentally measured values of G''. However, it still predicts values of G'' which are a factor of four to five lower than G', indicative of a material response that is primarily elastic at small strains.

In addition to the best fit provided by the solid line in Figs. 2 (a) and (b), we also illustrate sensitivity of the fit to slight variations in fitting coefficients, as well as sensitivity to experimental variability between data sets, by showing additional fits to the experimental data using dashed lines. For each data set (flowcurve or oscillatory shear data), the dashed line corresponds to parameters obtained by fitting the model to the other data set. The values of the fitting parameters are thus: flowcurve, solid line: $C/q = \sigma_y = 43$ Pa, $k = 19$ Pa.s^m, $m = 0.43$; flowcurve, dashed line: $C/q = \sigma_y = 43$ Pa, $k = 23$ Pa.s ^{m}, $m = 0.43$; oscillatory shear, solid line: $C/q = \sigma_y = 43$ Pa, $k = 23$ Pa.s^m, $m = 0.43$, $G = 200$ Pa, $q = 4$; oscillatory shear, dashed line: $C/q = \sigma_y = 43$ Pa, $k = 19$ Pa.s^m, $m = 0.43$, $G = 200$ Pa, $q = 12$. In general, we observe that the lower value of k used to fit the flowcurve data, results in a slight underprediction of the values of G'' and G' at large strains. This slight discrepancy

in this fitting coefficient is likely a result of experimental variability. The increase in q from a value of 4 to 12 (which appears to fit the Lissajous curves for this system best [30], and is hence used in Fig. 1) does not have any impact to the oscillatory shear data at large strains. However the increase from $q = 4$ to $q = 12$ does result in some changes to G' at moderate strains and to G'' at moderate to low strains. Despite these small differences, we see that in general, both sets of fitting coefficients capture the key trends observed in the Carbopol microgel

2.2. 3D version

The one-dimensional version of the KH model is useful for predicting material behavior under simple shearing conditions. For more complex flow scenarios, a more general constitutive framework is required. This framework must provide a constitutive law that is tensorial in nature, frame-invariant, and thermodynamically admissible. The relationship between the 3D version and 1D version of the KH model will therefore be analogous to that between the Upper Convected Maxwell (UCM) model and the simple scalar form of the Maxwell model (or that between the Oldroyd-B model and the Jeffreys model) [6].

A 3D version of the KH model has already been discussed in the appendix of [30], but we reproduce the formulation here because it forms the basis of the results which will follow. Throughout this section we will adopt the tensor notation of Gurtin et al. [5]. Because the KH model used here is a simplified version of the general elastoplastic formulations utilized by Anand et al. [43, 44, 45], it is fully frame invariant and thermodynamically admissible. For simplicity, we will omit some of the details presented in these earlier works that pertain to the issues of frame invariance and thermodynamic admissibility, and only discuss the key features of the KH model.

Kinematics. The 3D version of the KH model begins with the definition of the deformation gradient $\mathbf{F}$. The components of the deformation gradient are given by:

$$F_{ij} = \frac{\partial x_i}{\partial X_j}, \tag{18}$$

where (as discussed in Sec. 1) X_j are the cartesian components of the vector $\mathbf{X}$, which describes the position of material points in a body before a given deformation, and x_i are the cartesian components of the vector $\mathbf{x}$, which describes the position of the material points $\mathbf{X}$ after a given deformation.[4] Following the definition of the deformation gradient, the Kroner decomposition [46] can be used to decompose $\mathbf{F}$ into elastic and plastic contributions,

$$\mathbf{F} = \mathbf{F}^e\mathbf{F}^p \ . \tag{19}$$

The elastic part of the deformation gradient is further decomposed into the form

$$\mathbf{F}^e = \mathbf{R}^e\mathbf{U}^e \ , \tag{20}$$

where $\mathbf{R}^e$ is a rotation and $\mathbf{U}^e$ is a stretch. The elastic stretch $\mathbf{U}^e$ has a spectral representation

$$\mathbf{U}^e = \sum_{i=1}^{3} \lambda_i^e \mathbf{r}_i^e \otimes \mathbf{r}_i^e \ . \tag{21}$$

In the spectral representation of the elastic stretch $\mathbf{U}^e$, λ_i^e are the principal values and $\mathbf{r}_i^e$ are the principal directions of the elastic stretch tensor. The operator $\otimes$ indicates the dyadic product. Using $\mathbf{U}^e$, it is possible to define an elastic strain tensor which will be of use in specifying the elastic behavior of the material

$$\mathbf{E}^e \equiv \frac{1}{2}\left(\mathbf{F}^e(\mathbf{F}^e)^\intercal - \mathbf{1}\right) = \frac{1}{2}\left(\mathbf{U}^{e^2} - \mathbf{1}\right) \ . \tag{22}$$

Following [5], we name the above tensor $\mathbf{E}^e$ the Green-Saint Venant strain tensor.[5]

From a kinematical point of view, the time-differentiation of the Kroner decomposition in Eq. 19 allows for the velocity gradient, $\mathbf{L}$, to be written in terms of an elastic velocity gradient $\mathbf{L}^e$ and a plastic velocity gradient $\mathbf{L}^p$,

$$\mathbf{L} = \mathbf{L}^e + \mathbf{F}^e\mathbf{L}^p\mathbf{F}^{e^{-1}}, \tag{23}$$

[4] The deformation gradient $\mathbf{F}$ used here is identical to the "displacement gradient tensor" denoted as $\mathbf{E}$ in [6]. Here we reserve the use of the symbol $\mathbf{E}$ to describe the infinitesimal strain tensor defined in Sec. 1. Furthermore, in [6] the notation $\mathbf{r}$ is used in place of $\mathbf{x}$ and $\mathbf{r}'$ is used in place of $\mathbf{X}$

[5] According to [6], the tensor $\mathbf{E}^e$ would be called the "relative finite strain tensor" for the elastic part of the deformation gradient $\mathbf{F}^e$, and would be denoted as $-\frac{1}{2}\boldsymbol{\gamma}_{[0]}$ (see Eq. 8.1-9 in [6]). The tensor $\mathbf{F}^e(\mathbf{F}^e)^\intercal$ is also the Finger tensor of $\mathbf{F}^e$ (denoted as $\mathbf{B}$ in Eq. 8.1-7 in [6]).

where $\mathbf{L}^e$ and $\mathbf{L}^p$ are defined as follows:

$$\mathbf{L}^p \equiv \dot{\mathbf{F}}^p \mathbf{F}^{p^{-1}} \ , \tag{24}$$

$$\mathbf{L}^e \equiv \dot{\mathbf{F}}^e \mathbf{F}^{e^{-1}} . \tag{25}$$

The plastic velocity gradient $\mathbf{L}^p$ can be split into its symmetric and skew components such that $\mathbf{L}^p = \mathbf{D}^p + \mathbf{W}^p$. We call $\mathbf{D}^p$ the plastic stretching tensor (it is also sometimes referred to as the plastic deformation rate tensor) and $\mathbf{W}^p$ the plastic spin tensor. One of the assumptions in this model is that of plastic irrotationality, which takes $\mathbf{W}^p = 0$. This assumption is general and is justified in [5]. The plastic stretching $\mathbf{D}^p$ can also be written as a product of its magnitude, $d^p = |\mathbf{D}^p|$, and its direction $\mathbf{N}^p = \mathbf{D}^p/|\mathbf{D}^p|$.

$$\mathbf{D}^p = d^p \mathbf{N}^p \ . \tag{26}$$

Free energy. An important component of the KH model is the form of the free energy Ψ. We assume that the free energy consists of two separate terms: an elastic free energy Ψ^e, and a defect energy Ψ^p.

$$\Psi = \underbrace{G|\mathbf{E}^e|^2 + \frac{1}{2}\Lambda|\mathrm{tr}\mathbf{E}^e|^2}_{\text{elastic energy } \Psi^e} + \underbrace{\Psi^p(\mathbf{A})}_{\text{defect energy}} \ . \tag{27}$$

In Eq. 27 above, the parameter G is a shear modulus, and the parameter Λ is related to the bulk modulus K through $K = \Lambda + 2G/3$. The form of the elastic free energy results in the following relationship between the second Piola elastic stress $\mathbf{T}^e$ and the Green-St. Venant tensor $\mathbf{E}^e$:

$$\mathbf{T}^e = 2G\mathbf{E}^e + \Lambda\left(\mathrm{tr}\mathbf{E}^e\right)\mathbf{1} \ , \tag{28}$$

where $\mathbf{1}$ is the identity tensor. The second Piola elastic stress $\mathbf{T}^e$ is defined (and related to the Cauchy stress $\mathbf{T}$) as follows [5]:

$$\mathbf{T}^e \equiv J(\mathbf{F}^e)^{-1}\mathbf{T}(\mathbf{F}^e)^{-\intercal} \ , \tag{29}$$

where J is the determinant of the deformation gradient $\mathbf{F}$.

To define the defect energy $\Psi^p(\mathbf{A})$, we must first introduce the concept of the Mandel stress, which is defined as

$$\mathbf{M}^e \equiv J(\mathbf{F}^e)^\intercal \mathbf{F}^e \mathbf{T}^e = J(\mathbf{F}^e)^\intercal \mathbf{T} (\mathbf{F}^e)^{-\intercal} \ . \tag{30}$$

The Mandel stress is typically associated with an intermediate structural space in the material [5], and its deviatoric part is $\mathbf{M}_0^e = \mathbf{M}^e - \frac{1}{3}(\mathrm{tr}\mathbf{M}^e)\,\mathbf{1}$. Figure 3 (adapted from [5]) illustrates how the decomposition of the deformation gradient $\mathbf{F}$ results in three distinct "spaces" in which various tensor fields (e.g. stresses, deformation gradients) reside. These three spaces are the reference space, which is where the undeformed reference body resides, the observed space, which is where the deformed body resides, and an intermediate structural space. From the definition in Eq 30, it follows that the Mandel stress is a "structural tensor field" (according to the nomenclature of [5]) and therefore maps vectors in the structural space to other vectors in the structural space. It is used to define the defect energy in what follows, because it is dependent on changes to the material structure. The Mandel stress is related to, but distinct from the Cauchy stress (or true stress), which resides in the observed space of the deformed body.

The elastic energy Ψ^e is used to model purely reversible, elastic deformations within the material. The defect energy Ψ^p on the other hand, is introduced to model the structural rearrangement of the material's microconstituents. In the three dimensional KH formulation, Ψ^p depends on a strain-like tensor $\mathbf{A}$, which is analogous to the one-dimensional scalar internal variable A that was discussed in Sec. 2.1. The structural rearrangement that occurs when the material undergoes plastic flow can result from different underlying physical processes. In the case of metals, movement of dislocations cause a change in the defect energy. For foams and dense suspensions, topological rearrangement of bubbles or particles will cause the defect energy to change. Different elastoplastic materials will have different dependencies of the defect energy on the strain-like tensor $\mathbf{A}$. However, the basic form of Ψ given in Eq. 27, in which free energy is additively decomposed into a defect contribution and an elastic part, is general enough to describe a wide range of EVP materials.

For our purposes, we specify a very simple form of the defect energy Ψ^p. We first consider

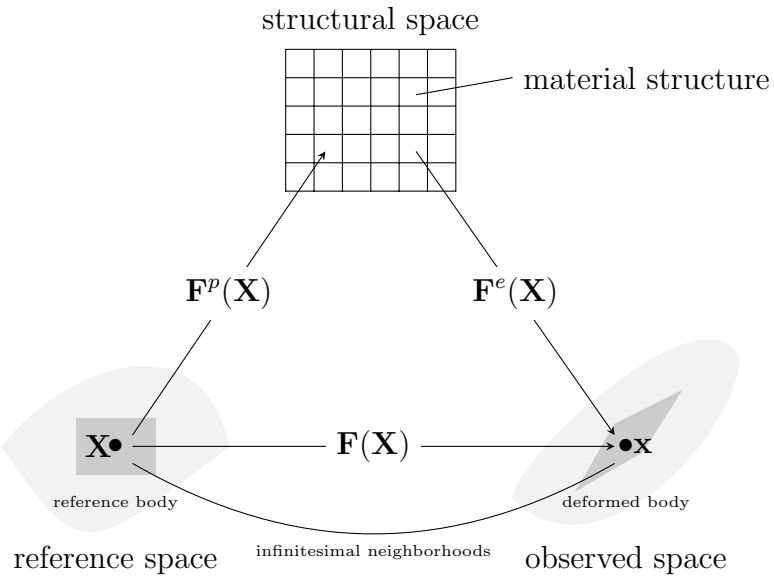

Figure 3: Diagram adapted from Gurtin et. al. [5] illustrating how the decomposition of the deformation gradient $\mathbf{F}$ results in three distinct spaces.

the spectral representation of the tensor $\mathbf{A}$:

$$\mathbf{A} = \sum_{i=1}^{3} a_i \mathbf{l}_i \otimes \mathbf{l}_i \ . \tag{31}$$

In the above equation, $\mathbf{l}_i$ are the principal directions of $\mathbf{A}$, and a_i are the principal values. The following form is employed for Ψ^p in the KH model [44, 45]:

$$\Psi^p = \frac{1}{4} C \left[(\log a_1)^2 + (\log a_2)^2 + (\log a_3)^2 \right] \ . \tag{32}$$

In Eq. 32 above the back stress modulus C has been introduced. Eq 32 above results in an expression for the back stress, which can be obtained by taking the derivative of Ψ^p with respect to $\mathbf{A}$ [44],

$$\mathbf{M}_{\text{back}} = C \log \mathbf{A} \ . \tag{33}$$

The tensor $\mathbf{A}$ is defined through an evolution equation [45]

$$\dot{\mathbf{A}} = \mathbf{D}^p \mathbf{A} + \mathbf{A} \mathbf{D}^p - q \mathbf{A} (\log \mathbf{A}) \dot{\bar{\gamma}}^p \ , \tag{34}$$

which is a generalized version of the Armstrong-Frederick kinematic hardening rule. Eq. 34 is typically evaluated with an initial condition of $\mathbf{A}$ equal to $\mathbf{1}$, the identity matrix, which

corresponds to a "virgin state" in the material [44, 45]. In Eq. 34 we have introduced the new material constant q (equivalent to the dimensionless q parameter discussed for the 1D model in Sec. 2.1). The parameter q governs the dynamic evolution of $\mathbf{A}$.

As was the case for the 1D KH model, we can write an effective stress

$$\mathbf{M}^e_{\text{eff}} = \mathbf{M}^e_0 - \mathbf{M}_{\text{back}} \ , \tag{35}$$

and constrain the plastic stretching to be codirectional to the effective stress

$$\mathbf{N}^p = \frac{\mathbf{M}^e_{\text{eff}}}{|\mathbf{M}^e_{\text{eff}}|} \ . \tag{36}$$

What now remains is to determine the magnitude of the equivalent plastic strain rate, d^p. We define an equivalent plastic strain rate and equivalent shear stress:

$$\dot{\bar{\gamma}}^p \equiv \sqrt{2} d^p \qquad \text{Equivalent plastic strain rate} \tag{37}$$

$$\bar{\sigma} \equiv \frac{1}{\sqrt{2}} |\mathbf{M}^e_{\text{eff}}| \qquad \text{Equivalent shear stress} \tag{38}$$

The $\sqrt{2}$ factors arise in the definitions of the equivalent quantities above so that under simple shearing flows, these quantities agree with the plastic shear rate $\dot{\gamma}^p$ and the stress σ used for the 1D (shear) version of the model introduced in Sec. 2.1. This will be made apparent in Sec. 2.3.1, where we obtain analytical expressions for the tensorial quantities of the 3D model under simple shearing flow, and relate them to predictions from the 1D version of the model.

After defining the equivalent shear stress and plastic strain rate, the power-law rate-dependent flow rule, which relates $\bar{\sigma}$ and $\dot{\bar{\gamma}}^p$, is specified:

$$\dot{\bar{\gamma}}^p = \left(\frac{\bar{\sigma}}{k} \right)^{1/m} \ . \tag{39}$$

This above flow rule has eliminated the conditionality that appears in many 3D generalizations of the Bingham or Herschel-Bulkley models [3, 13, 14]. The discontinuity in the plastic flow behavior has therefore been "regularized" through the introduction of the evolving tensor $\mathbf{A}$. Regularization of the yield criterion plays an important role in the numerical simulations of these types of constitutive laws [27, 25] - here it has been accomplished without explicitly specifying a finite, large constant viscosity below the yield stress.

2.3. 3D KH Model under steady flows

A viscometric flow commonly employed by rheologists is a steady simple shearing deformation, where the velocity gradient $\mathbf{L}$ is given as follows:

$$\mathbf{L} = \begin{bmatrix} 0 & \dot{\gamma} & 0 \\ 0 & 0 & 0 \\ 0 & 0 & 0 \end{bmatrix} \tag{40}$$

Rheologists will typically use such flows to determine the shear and normal stress components of the Cauchy stress tensor $\mathbf{T}$ for a complex fluid or soft solid, and then compare these measurements to predictions from constitutive laws. The 1-dimensional version of the KH model described and simulated in Sec. 2.1 only accounts for a single scalar shear stress. With the 3-dimensional form of the KH model outlined in the previous section, it is now possible to predict the full 3-dimensional form of the Cauchy stress tensor $\mathbf{T}$ for a number of different rheological flows including steady simple shear flow.

A rheologist will usually measure components of the Cauchy stress $\mathbf{T}$, in terms of the imposed stretching (or rate of deformation), $\mathbf{D}$. It is therefore necessary to obtain an analytical relationship of the form $\mathbf{T} = f(\mathbf{D})$ rather than of the form $\mathbf{T} = f(\mathbf{D}^p)$. To assist in obtaining such an expression, an assumption of *small elastic deformations* can be utilized. This assumption holds for a wide range of materials, and is valid when the yield stress $\sigma_y = C/q$ is much smaller than the elastic shear modulus G, i.e. the yield strain in shear is $\gamma_y \equiv C/(qG) \ll 1$. For a real EVP material, one can experimentally verify this criterion of small elastic strains by checking that the ratio $J'_M/\sigma_y \ll 1$. J'_M is a nonlinear LAOStress measure, called the tangent compliance, and is defined as

$$J'_M \equiv \left.\frac{d\gamma}{d\sigma}\right|_{\sigma=0}, \tag{41}$$

for an oscillatory shearing deformation where $\sigma = \sigma_0 \cos \omega t$ [30]. J'_M is generally representative of the elastic modulus of EVP materials, so if the constraint $J'_M/\sigma_y \ll 1$ is valid, then considerable plastic flow will be occurring at stresses which only cause small elastic deformations. From such an assumption, it follows that the elastic stretch tensor is very

close to the identity tensor, i.e. $\mathbf{U}^e \simeq \mathbf{1}$, and therefore from Eq. 20 $\mathbf{F}^e \simeq \mathbf{R}^e$. The elastic part of the deformation gradient $\mathbf{F}^e$ is now simply a rotation, for which its inverse is its transpose, $(\mathbf{R}^e)^{-1} = (\mathbf{R}^e)^\intercal$

Following this assumption, one can then obtain a simplified relation between the stretching tensor $\mathbf{D} = \frac{1}{2}(\mathbf{L} + \mathbf{L}^\intercal)$ and the plastic stretching tensor $\mathbf{D}^p$. The derivation is detailed in Appendix B.1, but we summarize it here:

$$\mathbf{D} = \mathbf{R}^e \mathbf{D}^p \mathbf{R}^{e^{-1}} \ . \tag{42}$$

The above equation can be used to obtain the following expression providing the rate of deformation tensor $\mathbf{D}$ in terms of the deviatoric Cauchy stress $\mathbf{T}_0 \equiv \mathbf{T} - \frac{1}{3}(\mathrm{tr}\mathbf{T})\,\mathbf{1}$ and a new internal parameter $\bar{\mathbf{A}}$ (the derivation for this step is also provided in Appendix B.1).

$$\mathbf{D} = \left(\frac{1}{\sqrt{2}} \left(\frac{|\mathbf{T}_0 - C \log \bar{\mathbf{A}}|}{\sqrt{2}k} \right)^{1/m} \frac{\mathbf{T}_0 - C \log \bar{\mathbf{A}}}{|\mathbf{T}_0 - C \log \bar{\mathbf{A}}|} \right) \ . \tag{43}$$

The tensor $\bar{\mathbf{A}} \equiv \mathbf{R}^{e^{-1}} \mathbf{A} \mathbf{R}^e$ in the equation above is an evolving internal parameter which lies in the space of the deformed body (illustrated in Fig. 3). $\mathbf{A}$, on the other hand, lies in the structural space of the body. The evolution equation for $\bar{\mathbf{A}}$ is now different from that of $\mathbf{A}$.

$$\overset{\circ}{\bar{\mathbf{A}}} = \mathbf{D}\bar{\mathbf{A}} + \bar{\mathbf{A}}\mathbf{D} - q\sqrt{2}\bar{\mathbf{A}} \log \bar{\mathbf{A}} |\mathbf{D}| \ . \tag{44}$$

Where $\overset{\circ}{\bar{\mathbf{A}}} = \dot{\bar{\mathbf{A}}} + \bar{\mathbf{A}}\mathbf{W} - \mathbf{W}\bar{\mathbf{A}}$ is the corotational derivative of $\bar{\mathbf{A}}$ [5] (and $\mathbf{W} = \dot{\mathbf{R}}^e \mathbf{R}^{e^{-1}}$ is the spin tensor). Alternatively Eq. 44 can be expressed in terms of the upper convected derivative of $\bar{\mathbf{A}}$ which is $\overset{\diamond}{\bar{\mathbf{A}}} = \dot{\bar{\mathbf{A}}} - \bar{\mathbf{A}}\mathbf{L}^\intercal - \mathbf{L}\bar{\mathbf{A}}$ [6]:

$$\overset{\diamond}{\bar{\mathbf{A}}} = -q\sqrt{2}\bar{\mathbf{A}} \log \bar{\mathbf{A}} |\mathbf{D}| \tag{45}$$

[6] According to [6] the notation that would be used for the upper-convected (or contravariant convected) derivative would be $\mathbf{A}_{(1)}$, while the notation used for the corotational (or Jaumann) derivative would be $\frac{\mathscr{D}}{\mathscr{D}t}\mathbf{A}$. Note that the definition of the velocity gradient tensor $\mathbf{L}$ used here (in accordance with [5]) is the same tensor as that denoted by $(\nabla \mathbf{v})^\dagger$ in [6]. See pg. 81 in [5] and pg. 296 in [6] for the definitions of the two tensors.

This evolution equation now involves a frame-invariant, corotational (or alternatively upper convected) derivative which accounts for the fact that $\bar{\mathbf{A}}$ lies in the deformed space of the body.

The two simple expressions, Eq. 45 and 43, analytically describe how the Cauchy stress $\mathbf{T}$ evolves in the material given a particular imposed deformation rate $\mathbf{D}$. These types of expressions can be used to understand the response of the material in an Eulerian reference frame, which is the basis for most rheological experiments. The only simplification that was made to arrive at these two equations was that of small elastic strains, i.e. $C/(qG) \ll 1$ (a reasonable assumption for many yielding materials), resulting in $\mathbf{U}^e \simeq \mathbf{1}$.

2.3.1. Steady shear

With Eqs. 45 and 43 derived, it is possible to obtain analytical expressions for the components of the Cauchy stress tensor $\mathbf{T}$ under steady shearing conditions as given in Eq. 40. For ease of representation, we rewrite Eq. 43 as follows

$$\mathbf{T}_0 = \sqrt{2}^{m+1} k|\mathbf{D}|^m \mathbf{N} + C \log \bar{\mathbf{A}}, \tag{46}$$

where $\mathbf{N}$ is the direction of stretching, defined as $\mathbf{N} = \mathbf{D}/|\mathbf{D}|$. To arrive at an analytical solution for the steady state values of the components of $\mathbf{T}$ under steady shear, we set $\dot{\bar{\mathbf{A}}} = 0$ in Eq. 45, and then solve for the steady state value of the tensor $\bar{\mathbf{A}}$ from the following equation:

$$\bar{\mathbf{A}}\mathbf{L}^{\intercal} + \mathbf{L}\bar{\mathbf{A}} - q\sqrt{2}\bar{\mathbf{A}} \log \bar{\mathbf{A}}|\mathbf{D}| = 0 \ . \tag{47}$$

Due to the presence of the $\bar{\mathbf{A}} \log \bar{\mathbf{A}}$ term in this equation, the individual components of $\bar{\mathbf{A}}$ are related through a set of nonlinear coupled equations. The equations can be linearized and simplified considerably for the case where $q \gg 1$. The initial conditions for imposition of steady shear are $\bar{\mathbf{A}}(t = 0) = \mathbf{1}$. For large values of q, the recovery or destruction term $-q\sqrt{2}\bar{\mathbf{A}} \log \bar{\mathbf{A}}|\mathbf{D}|$ grows quickly, resulting in $\bar{\mathbf{A}}$ being very close to $\mathbf{1}$ for all times. We can therefore use the substitution $\bar{\mathbf{A}} = \mathbf{1} + \mathbf{B}$, with $|\mathbf{B}| \ll 1$. The Mercator series for the natural logarithm of $\bar{\mathbf{A}}$ is as follows:

$$\log \bar{\mathbf{A}} = \log (\mathbf{1} + \mathbf{B}) = \mathbf{B} - \frac{\mathbf{B}^2}{2} + \frac{\mathbf{B}^3}{3} - \dots \tag{48}$$

Eq. 48 above can then be combined with Eq. 47. This results in the following expression:

$$2\mathbf{D} + \mathbf{B}\mathbf{L}^{\intercal} + \mathbf{L}\mathbf{B} - q\sqrt{2}|\mathbf{D}|\mathbf{B} = 0 + O(\mathbf{B}^2) \ . \tag{49}$$

Inserting a steady shear velocity gradient into the equation above (from Eq. 40), and keeping only terms that are linear in $\mathbf{B}$, gives the following relationship between the components of $\mathbf{B}$:

$$\begin{bmatrix} 0 & \dot{\gamma} & 0 \\ \dot{\gamma} & 0 & 0 \\ 0 & 0 & 0 \end{bmatrix} + \begin{bmatrix} 2\dot{\gamma}B_{12} & \dot{\gamma}B_{22} & 0 \\ \dot{\gamma}B_{22} & 0 & 0 \\ 0 & 0 & 0 \end{bmatrix} - q\dot{\gamma} \begin{bmatrix} B_{11} & B_{12} & 0 \\ B_{12} & B_{22} & 0 \\ 0 & 0 & 0 \end{bmatrix} \simeq 0 \ . \tag{50}$$

Solving this linear set of equations for the components of $\mathbf{B}$, gives the following values:

$$\mathbf{B} \simeq \begin{bmatrix} 2/q^2 & 1/q & 0 \\ 1/q & 0 & 0 \\ 0 & 0 & 0 \end{bmatrix} \ . \tag{51}$$

Next, using the fact that for $q \gg 1$, $\log \bar{\mathbf{A}} \simeq \mathbf{B}$, we can obtain the components of the deviatoric Cauchy stress tensor:

$$\mathbf{T}_0 \simeq \begin{bmatrix} 2\sigma_y/q & \sigma_y + k\dot{\gamma}^m & 0 \\ \sigma_y + k\dot{\gamma}^m & 0 & 0 \\ 0 & 0 & 0 \end{bmatrix} \ . \tag{52}$$

We therefore find that the 1-2 shear component of the deviatoric Cauchy stress is given by $T_{12} \simeq \sigma_y + k\dot{\gamma}^m$, which is the expected result for a Herschel-Bulkley type material with a shear yield stress $\sigma_y = C/q$. Note, however, that the expression for $\mathbf{T}_0$ in Eq. 52 is not strictly deviatoric, except in the limit where $q \to \infty$. This is due to the fact that the approximate solution above does not account for order $1/q^2$ terms in the 2-2 entry of $\log \bar{\mathbf{A}}$. This can be amended by taking higher order terms in the expansion of $\log \bar{\mathbf{A}}$. The resulting expressions obtained for the terms in $\log \bar{\mathbf{A}}$ are rather complex (and not included here). However, these expressions can be simplified by expansion through a Taylor series, resulting in terms up to order $1/q$ in the 1-2 component, and terms up to order $1/q^2$ for the 1-1 and

2-2 components. This yields the following expression for $\log \bar{\mathbf{A}}$:

$$\log \bar{\mathbf{A}} \simeq \begin{bmatrix} 1/q^2 & 1/q & 0 \\ 1/q & -1/q^2 & 0 \\ 0 & 0 & 0 \end{bmatrix} . \tag{53}$$

From which follows a better approximation for the now truly deviatoric Cauchy stress $\mathbf{T}_0$:

$$\mathbf{T}_0 \simeq \begin{bmatrix} \sigma_y/q & \sigma_y + k\dot{\gamma}^m & 0 \\ \sigma_y + k\dot{\gamma}^m & -\sigma_y/q & 0 \\ 0 & 0 & 0 \end{bmatrix} . \tag{54}$$

This KH model therefore predicts a first normal stress difference given by $N_1 \simeq 2C/q^2 = 2\sigma_y/q$, which is independent of the applied shear rate $\dot{\gamma}$. These normal stress differences arise in the absence of elastic stretches, because we have set $C/(qG) \ll 1$ to arrive at these expressions.

To confirm the validity of the expression in Eq. 54, and also investigate the range of q values over which it holds, we carried out numerical simulations in which Eqs. 45 and 43 were evolved under startup of a very small steady shear rate. The purpose of the small steady shear rate was to verify that the Cauchy stress evolves towards a point where $T_{12} \simeq C/q$ and where $N_1 \simeq 2C/q^2$ (as is given in Eq. 54). The shear rate $\dot{\gamma}$ is therefore chosen such that $(C/q) \gg k\dot{\gamma}^m$. Constitutive parameters identical to those used for the fitting of the Carbopol microgel in Sec. 2.1 were used (i.e. $C/q = \sigma_y = 45$ Pa, $m = 0.43$, $k = 23$ Pa.s^m) with the exception that G was set to infinity. The particular shear rate used was $\dot{\gamma} = 1 \times 10^{-3}$ s^{-1}, or in non-dimensional form, $\dot{\Gamma} \equiv \dot{\gamma} \left(\frac{C}{qk}\right)^{1/m} = 4.8 \times 10^{-3} \ll 1$. These simulations were carried out for a large range of q parameters, and the steady state values of both the dimensionless normal stress and shear stress (N_1/σ_y and T_{12}/σ_y respectively) are plotted below as a function of the dimensionless parameter q. As the results in Fig. 4 show, the approximate solution given by Eq. 54 predicts the values of T_{12} and N_1 for values of $q \gtrsim 4$. To improve the agreement at smaller values of q, higher order terms could be included in each component of $\mathbf{T}_0$.

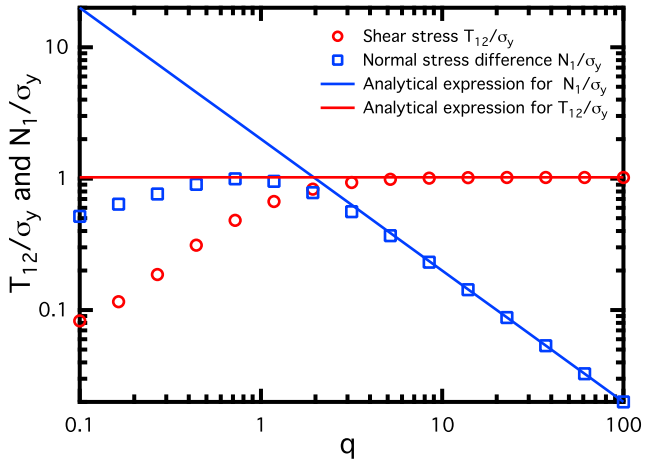

Figure 4: Plot of the simulated values (circles) of T_{12}/σ_y and N_1/σ_y for the 3D version of the KH model for a range of values for the q parameter. The solid lines show the prediction of these stresses obtained using the approximate solution in Eq. 54.

The relative magnitude of the normal stress difference observed in an elastoplastic yield stress fluid thus varies with the magnitude of the parameter q in the KH formulation. Increasing the q parameter, while keeping the shear yield stress σ_y constant, causes a decrease in the magnitude of the first normal stress difference N_1. However, q also affects the dynamics of the evolution equation of $\bar{\mathbf{A}}$. Specifically, larger values of q result in a quicker increase in the recovery term in the evolution equation for $\bar{\mathbf{A}}$. As a result, one would expect that the shear and normal stresses saturate to their steady values more quickly for large values of q. To illustrate this, we plot below the evolution in N_1/σ_y and T_{12}/σ_y vs. accumulated strain γ for the simplified 3D KH model (as given in Eq. 43 and 45) simulated under startup of steady shear at a shear rate of $\dot{\Gamma} = 4.8 \times 10^{-3}$. The same model parameters are used as in Fig. 4, and curves are plotted for seven different q values logarithmically spaced from 5 to 100. From Fig. 5 it is evident that larger values of q result in smaller strains accumulating before the stresses saturate. The factor $1/q$ therefore represents a critical strain required for the KH model to fully yield and evolve towards its steady state. Thus, this factor is effectively the yield strain of the KH framework. Since many yielding materials show yield at strains much smaller than unity, these derivations for the case when $q \gg 1$ are the most

practically relevant. The small values of the normal stress difference predicted in the limit $q \gg 1$ also help rationalize why robust experimental measurements of N_1 in yield stress fluids are difficult to make [47].

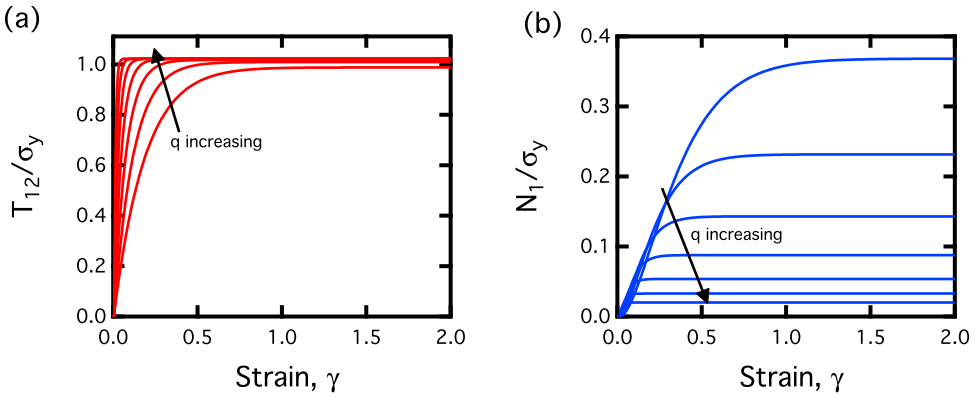

Figure 5: Plots of N_1/σ_y and T_{12}/σ_y vs. time for the 3D KH model simulated under startup of a steady shear rate of $\dot{\gamma} = 1 \times 10^{-3}$ s^{-1}. The same model parameters as in Fig. 4 are utilized, and curves are plotted for q values logarithmically spaced from $q = 5$ to $q = 100$ ($q = 5, 8, 14, 37, 61, 100$).

In the limiting case where $q \to \infty$, the first normal stress difference approaches zero and the shear stress T_{12} responds immediately to the imposition of a steady shear rate. In this limiting case, the behavior predicted by the KH model is identical to that of a Herschel-Bulkley ($m < 1$) or Bingham like ($m = 1$) model, with a von Mises yielding criterion to determine if plastic flow will occur. The case for $m = 1$ is identical to the inelastic version of the model introduced by Oldroyd [3], while the case of $m < 1$ and $q \to \infty$ is identical to the model used by Ovarlez et al. [13]).

The kinematic-hardening behavior therefore regularizes the flow/no flow condition in the Herschel-Bulkley model through the introduction of transient viscoplastic flow which can occur at all levels of stress. This is in contrast to regularization schemes which involve specifying Newtonian viscous flow with a very large viscosity for stresses below the yield stress σ_y [27]. This is an unrealistic assumption, because for many materials the apparent viscosity $\eta^+(t, \sigma_0)$ of the fluid varies in time when a stress is applied below σ_y, i.e. the material creeps before arresting. The limiting zero shear-rate viscosity of such materials is therefore not constant in time (or with increasing strain). The kinematic-hardening behavior

can also allow for partial elastic recoil to occur when the stress is stepped to zero after the material has undergone a creep test. This type of behavior cannot be accounted for in the 3 dimensional Herschel Bulkley type models used by Ovarlez et al. [13] or Martinie et al. [14].

2.3.2. Shear free flows

Uniaxial elongational flow. For elongational flow [6], the velocity gradient $\mathbf{L}$ takes the following form:

$$\mathbf{L} = \begin{bmatrix} \dot{\epsilon} & 0 & 0 \\ 0 & -\dot{\epsilon}/2 & 0 \\ 0 & 0 & -\dot{\epsilon}/2 \end{bmatrix} . \tag{55}$$

Following the same procedure outlined in Sec. 2.3.1 (i.e. neglecting order $\mathbf{B}^2$ terms and higher), a linear relationship between the components of $\mathbf{B}$ can be obtained:

$$\begin{bmatrix} 2\dot{\epsilon} & 0 & 0 \\ 0 & -\dot{\epsilon} & 0 \\ 0 & 0 & -\dot{\epsilon} \end{bmatrix} + \begin{bmatrix} 2B_{11}\dot{\epsilon} & 0 & 0 \\ 0 & -B_{22}\dot{\epsilon} & 0 \\ 0 & 0 & -B_{33}\dot{\epsilon} \end{bmatrix} - \begin{bmatrix} \sqrt{3}q\dot{\epsilon}B_{11} & 0 & 0 \\ 0 & \sqrt{3}q\dot{\epsilon}B_{22} & 0 \\ 0 & 0 & \sqrt{3}q\dot{\epsilon}B_{33} \end{bmatrix} \simeq 0 . \tag{56}$$

These components are solved and inserted into Eq. 46 (recall that $\log \bar{\mathbf{A}} \simeq \mathbf{B}$) to obtain an expression for the deviatoric Cauchy stress, $\mathbf{T}_0$.

$$\mathbf{T}_0 \simeq \begin{bmatrix} 2(\sqrt{3})^{m-1}k\dot{\epsilon}^m + \frac{2C}{\sqrt{3}q-2} & 0 & 0 \\ 0 & -(\sqrt{3})^{m-1}k\dot{\epsilon}^m - \frac{C}{1+\sqrt{3}q} & 0 \\ 0 & 0 & -(\sqrt{3})^{m-1}k\dot{\epsilon}^m - \frac{C}{1+\sqrt{3}q} \end{bmatrix} . \tag{57}$$

As was also the case in Eq. 52, the expression for $\mathbf{T}_0$ above is only deviatoric in the limit of large values of q. The diagonal terms in the equation for $\mathbf{T}_0$ above have power law terms proportional to $\dot{\epsilon}^m$, in addition to constant "yield terms" which contain the coefficients C and q. Using the expressions for the 1-1 and 2-2 components of $\mathbf{T}_0$, we write an approximate analytical expression for the extensional viscosity:

$$\eta_E \equiv \frac{T_{11} - T_{22}}{\dot{\epsilon}} \simeq \sqrt{3}^{m+1}k\dot{\epsilon}^{m-1} + \frac{3\sqrt{3}\sigma_y}{\dot{\epsilon}(3 - 2/q^2 - \sqrt{3}/q)} , \tag{58}$$

where we have substituted $\sigma_y = C/q$ to result in the order $1/q^2$ terms in the denominator. Considering the limit where $\dot{\epsilon} \to 0$, and $q \gg 1$, then the T_{11} stress component approaches a value of $2C/\sqrt{3}q$, while the T_{22} and T_{33} stress components approach values of $-C/\sqrt{3}q$. Under these conditions, the material will have just yielded. We insert the components of the stress tensor in this case into the von Mises yield criterion in order to determine an equivalent stress required for yielding

$$\sigma_e = \sqrt{\frac{(T_{11} - T_{22})^2 + (T_{22} - T_{33})^2 + (T_{11} - T_{33})^2 + 6({T_{12}}^2 + {T_{13}}^2 + {T_{23}}^2)}{2}}, \tag{59}$$

and obtain a value of $\sigma_e = \sqrt{3}C/q = \sqrt{3}\sigma_y$. This agrees with the equivalent stress σ_e determined for the simple shear case when $q \gg 1$. The material therefore yields under both shear and extensional deformations when the equivalent stress reaches the same value. This verifies that the KH model satisfies the von Mises yield criterion for large values of q. The von Mises yielding criterion has been experimentally verified for a wide range of EVP materials, including emulsions, physical gels and colloidal gels, among others [15, 13, 14].

To verify the validity of the approximation in Eq. 57, we plot in Fig. 6 the steady state, dimensionless normal stress difference ($N_1/\sigma_y = (T_{11} - T_{22})/\sigma_y$) against q for a very small dimensionless extensional strain rates ($\dot{\mathcal{E}} \equiv \dot{\epsilon}\left(\frac{C}{qk}\right)^{1/m} = 4.8 \times 10^{-3}$) under uniaxial elongational flow. In Fig. 6 we include the analytical approximation from Eq. 57 (solid line) as well as the direct numerical results obtained through numerical simulation of Eqs. 45 and 43 (hollow circles). There is good agreement between the analytical approximation and the numerical results for $q \gtrsim 8$. The numerical results generally predict a value of $N_1 \simeq \sqrt{3}\sigma_y$ in uniaxial extension for all values of q, so this appears to be a good approximation that holds even for smaller values of q. The analytical approximation, however, diverges at a value of $q = 2/\sqrt{3}$, and then becomes unphysical and negative for small values of q. While higher order terms of $\mathbf{B}$ can be used to obtain a more accurate approximation for $N_1(\dot{\epsilon})$, the results in Fig. 6 and the form of Eq. 58 suggest that the following expression for uniaxial extensional flow of the KH model holds over a large range of strain rates and q values:

$$N_1(\dot{\epsilon}) = \eta_E(\dot{\epsilon})\dot{\epsilon} \simeq \sqrt{3}^{m+1} k\dot{\epsilon}^m + \sqrt{3}\sigma_y \ . \tag{60}$$

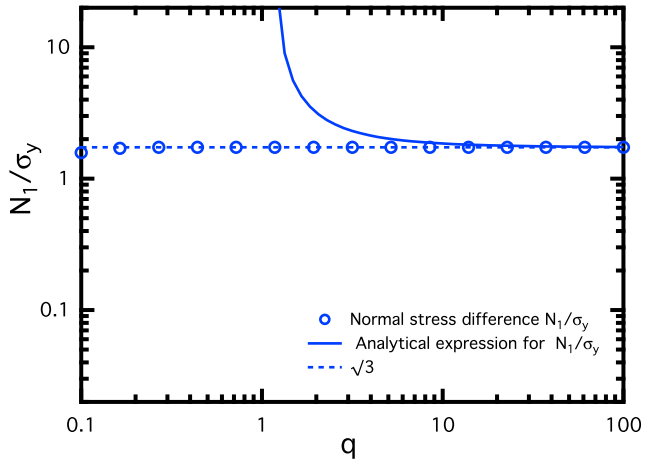

Figure 6: Plot of the simulated values (circles) of N_1/σ_y for the 3D version of the KH model for a range of values for the q parameter, under elongational flow at low deformation rates $\dot{\mathcal{E}} \ll 1$. The solid lines show the prediction of these stresses obtained using the approximate solution in Eq. 57.

Planar elongational flow. For planar elongational flow [6] the velocity gradient $\mathbf{L}$ takes the following form:

$$\mathbf{L} = \begin{bmatrix} \dot{\epsilon} & 0 & 0 \\ 0 & -\dot{\epsilon} & 0 \\ 0 & 0 & 0 \end{bmatrix} . \tag{61}$$

Combining the above equation with Eq. 49 gives the following relationship between the components of the tensor $\mathbf{B}$

$$\begin{bmatrix} 2\dot{\epsilon} & 0 & 0 \\ 0 & -2\dot{\epsilon} & 0 \\ 0 & 0 & 0 \end{bmatrix} + \begin{bmatrix} 2B_{11}\dot{\epsilon} & 0 & 0 \\ 0 & -2B_{22}\dot{\epsilon} & 0 \\ 0 & 0 & 0 \end{bmatrix} - \begin{bmatrix} 2q\dot{\epsilon}B_{11} & 0 & 0 \\ 0 & 2q\dot{\epsilon}B_{22} & 0 \\ 0 & 0 & 0 \end{bmatrix} \simeq 0 . \tag{62}$$

These can be solved for, and then inserted into Eq. 54 in order to obtain the components of the deviatoric Cauchy stress $\mathbf{T}_0$:

$$\mathbf{T}_0 \simeq \begin{bmatrix} k(2\dot{\epsilon})^m + \frac{C}{q-1} & 0 & 0 \\ 0 & -k(2\dot{\epsilon})^m - \frac{C}{q+1} & 0 \\ 0 & 0 & 0 \end{bmatrix} \tag{63}$$

The above result allows us to write the following approximation for the planar elongational viscosity (analogous to Eq. 58 above for the uniaxial elongational case)

$$\eta_P \equiv \frac{T_{11} - T_{22}}{\dot{\epsilon}} \simeq 2^{m+1} k \dot{\epsilon}^{m-1} + \frac{2\sigma_y}{\dot{\epsilon}(1 - 1/q^2)} \ . \tag{64}$$

For shear flow, elongational flow and planar elongational flow, the results giving the Cauchy stress tensor reduce to that of a Newtonian fluid with shear viscosity $\mu = k$ for the limits of $m = 1$, and $C/q = \sigma_y = 0$. As a result, the Trouton ratio for elongational flow will also approach $\eta_E/k = 3$ in this limit, and for planar elongational flow the Trouton ratio will approach $\eta_E/k = 4$.

2.3.3. Accounting for elastic deformations - large and small

Small elastic deformations. The simplifications so far of the equations in Sec. 2.2 have resulted in only the plastic part of the deformation gradient, $\mathbf{F}^p$, contributing to the total stretching deformation $\mathbf{D}$ of the material (this has resulted in the elastic modulus G not playing a role in the analytical results). It is possible to analytically account for *small* contributions to the deformation $\mathbf{D}$ from the elastic part of the deformation gradient, $\mathbf{F}^e$. In Eq. B.3, the assumption $\dot{\mathbf{U}}^e = 0$ was made. However if we account for a nonzero value of $\dot{\mathbf{U}}^e$, then the elastic part of the deformation gradient $\mathbf{L}^e$ can be rewritten:

$$\mathbf{L}^e = \underbrace{\dot{\mathbf{R}}^e \mathbf{R}^{e^{-1}}}_{\mathbf{W}^e, \text{ a spin}} + \underbrace{\mathbf{R}^e \dot{\mathbf{U}}^e \mathbf{U}^{e^{-1}} \mathbf{R}^{e^{-1}}}_{\mathbf{D}^e, \text{ a stretching}} \ . \tag{65}$$

Referring to the term $\mathbf{R}^e \dot{\mathbf{U}}^e \mathbf{U}^{e^{-1}} \mathbf{R}^{e^{-1}}$ as a stretching term only applies for small elastic deformations, when the skew part of $\dot{\mathbf{U}}^e \mathbf{U}^{e^{-1}}$ is close to zero (see pg. 90 of [5]). The elastic part of the deformation gradient now also has a stretching $\mathbf{D}^e$ in addition to the spin $\mathbf{W}^e$ (which was the only part of $\mathbf{L}^e$ accounted for in our assumptions thus far). Our total deformation $\mathbf{D}^t$ can now be written as a sum of two stretching deformations, $\mathbf{D}$ and $\mathbf{D}^e$

$$\mathbf{D}^t = \mathbf{D} + \mathbf{D}^e \ , \tag{66}$$

where $\mathbf{D} = \mathbf{R}^e \mathbf{D}^p \mathbf{R}^{e^{-1}}$, as given previously in Sec. 2.3, and $\mathbf{D}$ follows the same behavior as given earlier in Eqs. 45 and 43. Small elastic deformations can now be accounted for

by adding an additional elastic stretching $\mathbf{D}^e$ onto the plastic part of the stretching, $\mathbf{D} = \mathbf{R}^e\mathbf{D}^p\mathbf{R}^{e^{-1}}$. The additional elastic stretching $\mathbf{D}^e$ is related to a time derivative of the Cauchy stress $\mathbf{T}$. We take the time derivative of Eq. 28 to obtain the following:

$$\dot{\mathbf{T}}^e = 2G\dot{\mathbf{E}}^e + \Lambda(\mathrm{tr}\dot{\mathbf{E}}^e)\mathbf{1} \ . \tag{67}$$

By noting that $\overset{\circ}{\mathbf{T}} = \mathbf{R}^e\dot{\mathbf{T}}^e\mathbf{R}^{e^{-1}}$ (this again only holds for small elastic stretches), and also using the identity $\dot{\mathbf{E}}^e = \mathbf{F}^{e\intercal}\mathbf{D}^e\mathbf{F}^e \simeq \mathbf{R}^{e^{-1}}\mathbf{D}^e\mathbf{R}^e$ (see pg. 90 of [5]), we arrive at the following relation for the Cauchy stress:

$$\overset{\circ}{\mathbf{T}} = 2G\mathbf{D}^e + \Lambda\left(\mathrm{tr}\mathbf{D}^e\right) \ . \tag{68}$$

The relation above can also be inverted to give the elastic stretching $\mathbf{D}^e$ in terms of the corotational derivative of the Cauchy stress $\overset{\circ}{\mathbf{T}}$. The equation above allows one to account for the additional presence of small elastic stretches in the total deformation of the material.

Large elastic deformations. Obtaining an analytical expression for cases of large elastic stretches (i.e. $\mathbf{U}^e \gg \mathbf{1}$) is difficult, because the approximate relation $\mathbf{D} = \mathbf{R}^e\mathbf{D}^p\mathbf{R}^{e^{-1}}$ no longer holds. As a result, converting the tensorial form of the equations in 2.2 to an Eulerian reference frame involving $\mathbf{D}$ (or $\mathbf{D}^t$) is, to the authors' knowledge, not possible. However, numerical simulations on the set of equations given in Sec. 2.2 can be carried out. These are used to examine what the full 3D form of the KH model predicts when elastic stretches are large.

Startup of steady shear flow simulations were carried out using Matlab with the form of the equations given in Sec. 2.2 at a number of different imposed shear rates. The evolution on the components of the stress tensor $\mathbf{T}$ were monitored and the simulations were stopped when the tensor components approached steady state values. Plots of the dimensionless shear stress T_{12}/σ_y and the dimensionless first normal stress difference N_1/σ_y against applied dimensionless shear rate $\dot{\Gamma} \equiv \dot{\gamma}\left(\frac{C}{qk}\right)^{1/m}$ are given below in Fig. 7. The particular fitting coefficients used for this 3D simulation of the full form of the KH model are consistent with those used for a previous study of Carbopol microgels [30]. Specifically: $C/q = \sigma_y = 45$ Pa,

$m = 0.43$, $k = 23$ Pa.s^m, $q = 12$, and $G = 350$ Pa. The full 3D form of the KH model in Sec. 2.2 also requires specifying the parameter Λ. We set $\Lambda = 5000$ Pa, so that $C/(q\Lambda) = 0.01 \ll 1$ and the material's elastic behavior approaches that of an incompressible solid . Overlaid on the values corresponding to this simulated flowcurve in Fig. 7 are the analytical prediction for the shear stress from Eq. 54 (which assumed $q \gg 1$ and $C/(qG) \ll 1$).

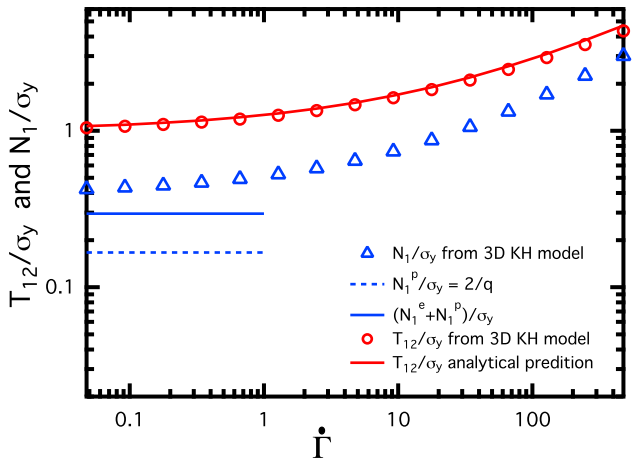

Figure 7: Prediction of the steady flowcurve for the 3D form of the KH model given in Sec. 2.2. Circles give the predicted dimensionless shear stress and triangles indicate the computed first normal stress difference. The solid lines are predictions using the analytical approximations in Eq. 54.

The analytical expression for the shear stress T_{12} is the same as the 1-D Herschel-Bulkley equation, and it agrees with the predictions of the simulation. This shows that the 3D form of the KH model is a more general form of the 1-D version discussed in Sec. 2.1. It also implies an equivalency between the parameters fitted using the 1-D version of the model, and the parameters that must be provided to the 3D formulation. This makes fitting experimental flowcurve data (such as that in Fig. 2 (a)) to the 3D form of the KH model very simple.

At the lowest shear rates $\dot{\Gamma}$, one can make an *a posteriori* estimate of the order of magnitude of elastic stretches (γ^e). A rough estimate gives $\gamma^e \sim T_{12}/G \sim C/(qG) = 0.13$, which is still well below unity. At the highest shear rates $\dot{\Gamma} \geq 100$, the analytical expression for T_{12} slightly over-predicts the values obtained from simulations of the full 3D form of the KH model. At these highest shear rates, we estimate the elastic stretches to be $\gamma^e \sim 0.58$,

which are nearing a value of 1. However, there is only a 7.5% disagreement between the analytical expression for T_{12} from Eq. 54 and the simulated value of T_{12} at these high shear rates.

From Fig. 7, it is clear that the values of N_1 are under-predicted by the analytical rate independent approximation in Eq. 54. The analytical expression in Eq. 54, which was derived assuming small elastic deformations, offers a lower bound on the value of N_1. When there are large elastic deformations ($C/(qG) \gg 1$), a large additional contribution towards the total first normal stress difference N_1 will come from nonlinearities arising in the elastic stress-strain relation specified in Eq. 28. For shear rates that approach zero, one can estimate the contribution to N_1 from the elastic-stress strain relation (we call this contribution N_1^e). This can be done by noting that for the case of simple shear with magnitude γ in the 1-2 entry in the elastic part of the deformation gradient $\mathbf{F}^e$, the form of the elastic free energy in Eq. 28 predicts a normal stress difference $T_{11} - T_{22} = G\gamma^2$. Under steady shear where the material has yielded, the extent of elastic shear strain accumulated γ can be estimated as σ_y/G, which is essentially the "yield strain" of the material. This contribution to N_1 is therefore $N_1^e = \sigma_y^2/G = C^2/(q^2G)$. This estimate also underpredicts the simulated value of N_1 provided in Fig. 7, suggesting that the actual value of N_1 consists of contributions from both the defect energy Ψ^p and the elastic free energy Ψ^e. When these contributions are added as per the following equation:

$$N_1 \simeq N_1^p + N_1^e = \frac{2\sigma_y}{q} + \frac{\sigma_y^2}{G}, \tag{69}$$

the prediction approaches the simulated value of N_1 at low shear rates. This demonstrates that the functional form of N_1 can be tuned by altering the expression which gives the elastic free energy, e.g. introducing a linear elastic, neo-Hookean or Mooney-Rivlin solid [7, 5]. This provides additional flexibility within the framework of the KH model to describe the elastic response of real elastoviscoplastic (EVP) materials, however, the predictions for $N_1(\dot{\gamma})$ must then be obtained numerically.

2.4. Further discussion

2.4.1. Oldroyd-B model vs. KH model

The form of the KH model discussed in Sec. 2.3 is very similar to the Oldroyd-B constitutive model that is often used to describe polymer melts and solutions. The Oldroyd-B model is equivalent to an upper convected Jeffreys model [6], in which the total stress in the material is additively decomposed into a polymeric contribution $\mathbf{T}_p$ and a solvent contribution $\mathbf{T}_s$, as follows:

$$\mathbf{T} = \underbrace{2\eta_s \mathbf{D}}_{\mathbf{T}_s} + \underbrace{G_p(\hat{\mathbf{A}} - \mathbf{1})}_{\mathbf{T}_p} \ . \tag{70}$$

With G_p a modulus and η_s a viscosity coefficient. The tensor variable $\hat{\mathbf{A}}$, much like the $\bar{\mathbf{A}}$ tensor used by the KH model in Sec. 2.3, is an internal strain-like microstructural variable which evolves according to the following differential equation:

$$\dot{\hat{\mathbf{A}}} = \mathbf{L}\hat{\mathbf{A}} + \hat{\mathbf{A}}\mathbf{L}^{\intercal} - \frac{G_p}{\eta_p}(\hat{\mathbf{A}} - \mathbf{1}) \ . \tag{71}$$

Eq. 71 above can be derived from considering a dilute suspension of linearly elastic dumbbells [48]. The tensor $\hat{\mathbf{A}} = \langle \mathbf{QQ} \rangle / {Q_0}^2$ represents the second moment tensor of the dumbbell distribution, and the relaxation time scale for the dumbbells is given by $\tau_p = \eta_p / G_p$

Revisiting the form of the KH model discussed in Sec. 2.3, we can decompose the deviatoric Cauchy stress for our elastoviscoplastic material in a manner similar to Eq. 70. However for the KH model, the viscous solvent term $\mathbf{T}_s$ becomes replaced by an inelastic or generalized Newtonian fluid term, while the polymeric contribution to stress (which results from deformation of the material microstructure) becomes the back stress, $\mathbf{T}_{\text{back}}$:

$$\mathbf{T}_0 = \underbrace{\sqrt{2}^{m+1} k |\mathbf{D}|^m \frac{\mathbf{D}}{|\mathbf{D}|}}_{\mathbf{T}_s} + \underbrace{C \log \bar{\mathbf{A}}}_{\mathbf{T}_{\text{back}}} \ , \tag{72}$$

where the tensor $\bar{\mathbf{A}}$ evolves according to the following differential equation:

$$\dot{\bar{\mathbf{A}}} = \mathbf{L}\bar{\mathbf{A}} + \bar{\mathbf{A}}\mathbf{L}^{\intercal} - \sqrt{2} q |\mathbf{D}| \bar{\mathbf{A}} \log \bar{\mathbf{A}} \ . \tag{73}$$

Eqs. 72-73 are similar to the Oldroyd-B model if we set $m = 1$ and consider large values of q. When q is large, we can approximate both the $\log \bar{\mathbf{A}}$ terms and the $\bar{\mathbf{A}} \log \bar{\mathbf{A}}$ terms as

$(\bar{\mathbf{A}} - \mathbf{1})$. This results in the following expressions for the Cauchy stress, and the evolution equation for $\bar{\mathbf{A}}$ for the KH model in the limit $q \gg 1$:

$$\mathbf{T}_0 = \underbrace{2k\mathbf{D}}_{\mathbf{T}_s} + \underbrace{C(\bar{\mathbf{A}} - \mathbf{1})}_{\mathbf{T}_{\text{back}}} \ , \tag{74}$$

$$\dot{\bar{\mathbf{A}}} = \mathbf{L}\bar{\mathbf{A}} + \bar{\mathbf{A}}\mathbf{L}^{\intercal} - \sqrt{2}q|\mathbf{D}|(\bar{\mathbf{A}} - \mathbf{1}) \ . \tag{75}$$

Eqs. 74 and 75 now appear identical to the equations for the Oldroyd-B constitutive law, with the one exception that the relaxation rate $1/\tau_p = G_p/\eta_p$ in front of the recovery term in Eq. 71 has been replaced by $\sqrt{2}q|\mathbf{D}|$. This is equivalent to a White-Metzner approximation in which the polymeric relaxation time τ_p in the Oldroyd-B model is a function of the magnitude of the strain rate tensor $|\mathbf{D}|$. Due to the specific functional form chosen for this relaxation time ($\tau_{KH} = 1/(\sqrt{2}q|\mathbf{D}|)$) the relaxation time diverges in the limit of slow flows. This simple modification causes a yielding behavior to arise.

This comparison of the Oldroyd-B model and the KH model is best illustrated visually through a diagram of mechanical analog elements as shown in Figs. 8 (a) and (b). The mechanical analog element for the KH model is drawn for the limiting case of $m = 1$, $q \gg 1$ and $C/(qG) \to 0$. In Fig. 8, the elements for the two models are arranged in a similar fashion, with two branches resulting in the stress being additively decomposed into two components. For the case of the KH model, however, the polymer contribution to the stress $\mathbf{T}_p$ is replaced by the back stress, $\mathbf{T}_{\text{back}}$. Table 1 shows the parameter equivalency between the KH model and the Oldroyd-B model. This equivalency only holds for the KH model framework when $m = 1$, $q \gg 1$ and $C/(qG) \ll 1$.

In order to account for elastic deformations in the KH model, it is necessary to include another elastic element with modulus G in series with this Jeffreys type element. When such an element is added, the mechanical analog then becomes identical to that which is discussed in Sec. 2.1, where predictions of the linear viscoelastic moduli were given for the one dimensional version of the model when $m = 1$. This is due to the fact that at small deformations, $|\mathbf{D}|$ approaches zero, which results in an infinite viscosity for the dissipative element in the back stress branch.

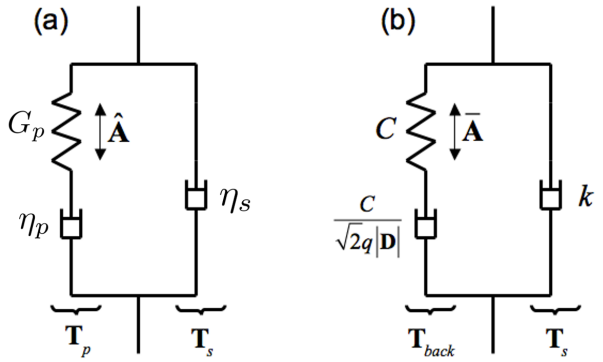

Figure 8: Mechanical analog element for the Oldroyd-B model (a) and the KH model (b). The mechanical analog element for the KH model is drawn for the limiting cases of $m = 1$, $q \gg 1$ and $C/(qG) \ll 1$.

Table 1: Table showing the parameter equivalency between the KH model framework and the Oldroyd-B model (here the KH model is simplified for the limiting case where $m = 1$, $q \gg 1$ and $C/(qG) \ll 1$).

	3DKH (for $m = 1$, $q \gg 1$ and $C/(qG) \to 0$)	Oldroyd-B
Solvent Viscosity	k	η_s
Modulus	C	G_p
Polymer Viscosity	$\frac{C}{\sqrt{2q}\|\mathbf{D}\|}$	η_p
Relaxation Time	$\tau_{KH} = \frac{1}{\sqrt{2q}\|\mathbf{D}\|}$	$\tau_p = \frac{\eta_p}{G_p}$
Internal Variable	$\bar{\mathbf{A}}$	$\hat{\mathbf{A}}$
Back/Polymer Stress	$\mathbf{T}_{\text{back}}$	$\mathbf{T}_p$

The use of modified Jeffreys-like constitutive laws to describe yielding behaviors is common in the rheology literature. The models used by Coussot et al. [49], Quemada [50], Dullaert and Mewis [51] and Souza Mendez [52] are variants of the Jeffreys model (and most of these are cast into one dimensional forms). The model introduced by Saramito [20, 21] is not built up using the Jeffreys model as a starting point, but can still be represented using simple mechanical analog elements, and with the correct modifications, can be converted into a representation such as the model discussed here. Indeed, recent work by Fraggedakis [38] implemented the kinematic hardening mechanism discussed here into the Saramito model. This implementation improved the agreement of the model predictions to experimental measurements of G' and G'' for a carbopol microgel over a wide range of frequencies and strains.

In summary, the unique aspect of the KH model framework is that with the modification of one model parameter in the Jeffreys model, η_p, the KH constitutive law can predict a yield-like behavior, slow viscoplastic creepeing flow, and the correct material behavior as it transitions from an unyielded to a yielded state under large amplitude oscillatory flows [30, 31, 38]. This is perhaps simpler and more intuitive than the modifications made in the other models mentioned here, however these more complex models are also designed to account for thixotropic effects. Thixotropy is often prevalent in EVP materials, so in the following section we discuss how to implement thixotropic behavior into the KH model framework.

2.4.2. Implementing thixotropy

The KH model framework as presently formulated does not account for thixotropic behavior. Thixotropic effects are typically manifested as an aging and shear rejuvenation behavior [53]. Rheological aging behavior is usually associated with Brownian motion and thermally attracted rearrangement of a material's microconstituents, even in the absence of shear. The internal parameter $\mathbf{A}$ in the KH model only evolves under the application of a non-zero shear rate $\dot{\bar{\gamma}}^p$, so aging behavior will not be predicted by the model.

There are a number of phenomenological approaches to modify the KH model to account

for the thixotropic behavior which is frequently observed in EVP materials [53, 54]. Most of these methods involve introducing a positive scalar internal variable, λ, which is a dimensionless, scaled measure of the internal state of the material order. This parameter then evolves with deformation according to a differential equation. This equation must account for both aging and shear rejuvenation. The KH model parameters can then be specified as a function of λ. For example, the viscosity k can be related to λ so that it decreases when the material shear rejuvenates, and increases when the material ages. This is the approach taken in the works by Coussot et al. [49] Quemada [50], Dullaert and Mewis [51] and Souza Mendez [52]. Another approach would modify the scalar flow rule in Eq. 39 in order to account for the presence of a scalar yield stress. This scalar yield stress is dependent on the level of structure in the material, which again is captured by the parameter λ. The appropriate flow rule thus becomes:

$$\dot{\bar{\gamma}}^p = \left(\frac{\bar{\sigma} - \sigma_y}{k} \right)^{1/m} \qquad \text{if } \bar{\sigma} > \sigma_y \text{ , } \dot{\bar{\gamma}}^p = 0 \text{ otherwise} \tag{76}$$

$$\sigma_y = \sigma_y(\lambda) \tag{77}$$

These equations allow the material to *isotropically* harden and soften. This is in contrast to the process of *kinematic* hardening, in which the material may strengthen along the direction of deformation, i.e. in a non-isotropic manner. Constitutive laws which account for both isotropic and kinematic hardening allow for both the size and center of the yield surface (in stress space) to vary, and may thus be referred to as isotropic-kinematic hardening (IKH) models [31, 32].

2.4.3. The importance of thermodynamic admissibility

Although the KH model framework offers flexibility in implementing thixotropic behavior, we emphasize that there are thermodynamic restrictions to the types of modifications that are allowable. Many workers have utilized models which specify a dependency of a modulus (e.g. G) on the structural parameter (e.g. λ) - see for example, Quemada [50], Dullaert and Mewis [51], Souza Mendez [52] and Mujumdar et. al. [55]. Without careful treatment, this type of dependency, combined with rheological aging in the material, may

violate dissipation inequalities that are derived through the first and second laws of thermodynamics. Gurtin et. al. [5] give the following mechanical free energy imbalance for an isothermal material:

$$\mathbf{T} : \mathbf{D} - \dot{\Psi} = \delta \geq 0 \ , \tag{78}$$

where Ψ is the free energy per unit volume in the material, and δ is the overall dissipation in the material per unit volume, which is always non-negative. Consider a Jeffreys type viscoelastic model, where the solvent viscosity is set to $\eta_s = 0$ and the polymer viscosity is set to $\eta_p \to \infty$, leaving a single elastic element with modulus $G(\lambda)$. For simple 1-D deformations, $\Psi = G(\lambda)\gamma^2/2$, with G an increasing function of λ. The aging process causes an increase in λ under a zero shear rate, so it is possible for $\dot{\lambda}$ (and $\dot{\Psi}$) to be positive when $\mathbf{D}$ or $\dot{\gamma}$ are zero. Therefore, the left hand side of Eq. 78 will be negative during this aging process, violating the dissipation inequality.

To illustrate how such models give unphysical predictions, we consider the following sequence of step deformations (which have been discussed previously in [34, 56]) for this type of "thixoelastic" element with $\sigma = G(\lambda)\gamma$: First, a step in strain of amplitude γ_0 is imposed at $t = t_1$. At this initial time, the material is not in its fully aged state with $G(\lambda) = G_1$, a low value. The stress will increase instantaneously to a value of $\sigma(t_1) = G_1\gamma_0$. The material is then allowed to age (i.e. the parameter λ increases) while the strain is held constant, resulting in the modulus increasing to a new, larger value $G(\lambda) = G_2$. This results in the stress in the material increasing to preserve the equality $\sigma = G(\lambda)\gamma_0$. At some time t_2, the strain is stepped down to zero, which also results in the stress stepping down to zero. The sequence of steps in strain and stress are shown graphically in the figure below:

The mechanical work done on the material for each step in strain, W_1 and W_2 can be evaluated through the following integrals:

$$W_1 = \int_{t_1^-}^{t_1^+} \sigma(t)\dot{\gamma}(t)dt = \frac{G_1\gamma_0^2}{2} \ , \tag{79}$$

$$W_2 = \int_{t_2^-}^{t_2^+} \sigma(t)\dot{\gamma}(t)dt = -\frac{G_2\gamma_0^2}{2} \ . \tag{80}$$

In this thixoelastic element $G_2 > G_1$, so the material returns more energy than what was

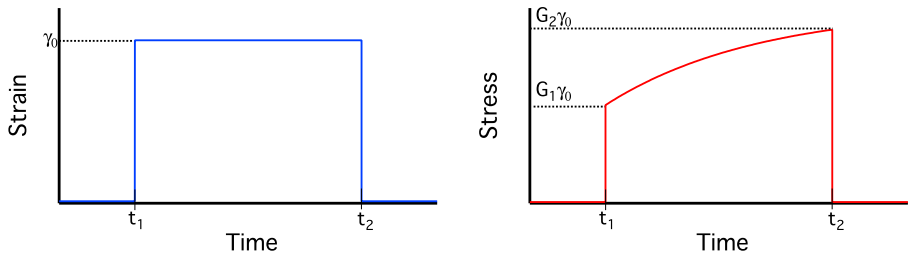

Figure 9: Sequence of steps in strain on a purely "thixoelastic" element with $\sigma = G(\lambda)\gamma$. The aging results in an increase in stress while the strain is held constant. This allows the material to increase the energy it has stored, while the extent of its deformation remains constant.

initially input and stored elastically at $t = t_1$. This is unphysical, and a more sophisticated constitutive formulation is required in order to correctly capture this thixoelastic behavior. Such a model must begin from specifying a form of the free energy in the material Ψ, so as to not violate forms of the dissipation inequality such as that given by Eq. 78. This form of the free energy must correctly account for the effect that aging has on the material, and may necessarily need to be cast as a thermomechanically coupled model due to the underlying thermal/Brownian mechanisms which are responsible for the aging process. Representative formulations which have explicitly ensured the correct free energy imbalance include those used by Anand et al. [43] from the plasticity literature, and Wei et al. [37], which are more recent additions from the rheology literature.

3. Conclusions

We have proposed a comprehensive framework for modeling elasto-viscoplastic behavior in complex fluids. This framework is rooted in the approach taken in plasticity, where deformations are decomposed systematically into reversible (elastic) and irreversible (plastic) components.

Two different versions of a "kinematic hardening" model have been discussed here. A simple one-dimensional version, and a three-dimensional, frame invariant, thermodynamically consistent version. The 3D formulation is analogous to how the UCM or Oldroyd-B models represent general frame-invariant formulations of the linear Maxwell and Jeffreys

models respectively [6]. We also demonstrated an equivalency between the model parameters of the 3D frame invariant form of this KH model, and the 1D form.

Predictions of this KH model for several canonical rheological flows (steady shear, uniaxial and planar extension) were considered, and analytical expressions of the tensor valued Cauchy stress were derived under certain limiting conditions corresponding to small elastic deformations. Predictions were also provided for different rheological experiments (steady flowcurve, creep, SAOS). and the model was fitted to experimental data for a model yield stress fluid (a Carbopol microgel).

The 3D KH formulation can be simplified to other constitutive laws under certain limits. Specifically, for the limit $\sigma_y \to 0$, the 3D KH model simplifies to a generalized Newtonian fluid model with either a constant Newtonian viscosity, or power law rheology, depending on the value of m. In the limit of $q \to \infty$, the 3D KH model simplifies to a 3D Bingham or Herschel Bulkley like viscoplastic fluid (again depending on the value of m) with a von Mises yielding criterion which determines whether plastic flow will occur or not. In the limit $q \gg 1$, the expression for the yield stress $\sigma_y = C/q$ was shown to represent a material with a (back stress) modulus C and a yield strain $\gamma_y \simeq 1/q$.

The similarities between the frame-invariant Oldroyd-B model and the 3D KH model were also illustrated. The KH framework can be likened to a White-Metzner generalization of the upper-convected Jeffreys model in which the relaxation time has a specific functional form $\tau_{KH} = 1/(\sqrt{2}q|\mathbf{D}|)$. We ended with a discussion of two important current aspects of modeling TEVP behavior. First, how to implement thixotropy into this framework, and secondly, how to keep these models thermodynamically admissible as they are modified to describe the response of real materials.

We conclude by reiterating the many benefits of this constitutive framework. First, the framework discussed here is fully 3D, frame invariant, and thermodynamically admissible. This is useful for conducting simulations of soft materials under complex flow scenarios. Second, the framework is flexible because it can allow the introduction of more complex behavior, such as thixotropy, different types of kinematic hardening, and variants of viscoelastic behavior below yield to predict normal stresses and other aspects of nonlinear

elasticity.

Compared to the commonly used generalization of the Bingham or Herschel-Bulkley model [3] the KH model offers several improvements. First, the flow/no flow criterion is regularized using the evolution equation for $\mathbf{A}$. This lets the material naturally evolve towards a yielded or unyielded state, depending on the level of the stress that develops in the material under an imposed deformation. Consequently, there is no need to track yield surfaces (in physical space) when simulating flow transients of the 3D KH model in more complex geometries. Secondly, the KH model is able to predict transient creeping flow for stresses below the yield stress σ_y. These types of transients are commonly observed in EVP materials, and a single large zero shear rate viscosity parameter is not sufficient to characterize this behavior. Third, tuning of the elastic material response in the 3D KH model can be used to capture the range of normal stress difference responses observed in real in EVP materials. Fourth, and finally, the KH model is generally able to capture material behavior over a much larger range of rheological experiments (e.g. LAOS, creep behavior). All of this is accomplished with the introduction of one additional fitting parameter, the coefficient q, and an evolution equation for the internal variable $\mathbf{A}$.

Acknowledgments

The authors would like to acknowledge L. Anand and K. Kamrin for help with developing the constitutive model. They would also like to thank Dr. Will Hartt and Lori Bacca of Procter and Gamble for providing the Carbopol samples. C.J.D. also acknowledges A. M. Osorno for fruitful discussions, and Chevron Energy Technology Corporation for providing funding.

Appendix A. Predictions of 1D KH model

Appendix A.1. Derivation of creep behavior of KH model

An expression for the asymptotic, long time dependency of strain on time for the KH model undergoing creep can be obtained by assuming the following time-varying form for

the internal structure parameter A

$$A \simeq \frac{\sigma_0}{C} - \frac{b}{t^x} \ , \tag{A.1}$$

where b is an unknown prefactor, and x is an unknown exponent. Taking the derivative of Eq. A.1 results in an expression for $\dot{A}$

$$\dot{A} \simeq \frac{bx}{t^{x+1}} \ . \tag{A.2}$$

Substituting Eq. A.1 into Eqs. 6 and 9, and then combining these two expressions yields another expression for $\dot{A}$

$$\dot{A} \simeq \left(\frac{Cb}{kt^x}\right)^{1/m} \left(1 - \frac{q\sigma_0}{C}\right) \ . \tag{A.3}$$

When inserting Eq. A.1 into Eqn. 9, we approximate $\dot{\gamma}^p(1 - qA(t))$ as $\dot{\gamma}^p(1 - q\sigma_0/C)$. Comparing the exponents and prefactors in Eq. A.3 with those of Eq. A.2 gives the following expressions for x and b

$$x = \frac{m}{1-m} \ , \tag{A.4}$$

$$b = \left[\left(1 - \frac{q\sigma_0}{C}\right)\left(\frac{1-m}{m}\right)\right]^{\frac{m}{m-1}} \left(\frac{C}{k}\right)^{\frac{1}{m-1}} \ . \tag{A.5}$$

The expressions above can be inserted into either Eq. A.3 or A.2, which can in turn be inserted into Eq. 6. This results in an expression for the rate of plastic strain $\dot{\gamma}^p$. This can be used to determine the apparent viscosity $\eta^+ \equiv \sigma_0/\dot{\gamma}^p$, which is as follows

$$\eta^+ \simeq \eta_c \left(\frac{t}{t_c}\right)^{1/(1-m)} \ , \tag{A.6}$$

where t_c is the characteristic time scale in Eq. 12 and η_c is the characteristic viscosity scale in Eq. 13.

Appendix A.2. Derivation of SAOS behavior of KH model ($m = 1$)

For SAOS, an oscillatory shear stress $\sigma = \sigma_0 \cos \omega t$ is imposed with $\sigma_0 \ll \sigma_y = C/q$. The magnitude of the terms on the right hand side of Eq. 9 can be compared, and since

$qA \ll 1$ the second term can be ignored. As a result, A can be approximated by the following differential equation:

$$\dot{A} \simeq \dot{\gamma}^p \ . \tag{A.7}$$

For small oscillatory stresses, integration from a fully relaxed equilibrium gives $A \simeq \gamma^p$. Inserting this (and the expression $\sigma = \sigma_0 \cos \omega t$) into Eq. 6 (while taking account of the directional integer n^p) then gives the following first order linear ODE:

$$\dot{\gamma}^p + \frac{C}{k}\gamma^p = \frac{\sigma_0}{k} \cos \omega t \ . \tag{A.8}$$

The above equation can be solved using an integrating factor, resulting in the following expression for $\gamma(t)$:

$$\gamma = \sigma_0 \left(\frac{1}{G} + \frac{C}{C^2 + k^2\omega^2} \right) \cos \omega t + \sigma_0 \left(\frac{k\omega}{C^2 + k^2\omega^2} \right) \sin \omega t \ . \tag{A.9}$$

In Eq. A.9, the total (measurable) strain in the material $\gamma = \gamma^e + \gamma^p$ is given, so a term with the elastic modulus G enters directly into the resulting expression for the strain (and this term is in phase with the driving sinusoidal stress).

The coefficients in front of the cosine and sine terms in the parentheses in Eq. A.9 above are the linear viscoelastic compliances $J'(\omega)$ and $J''(\omega)$ respectively. These can be converted to the linear viscoelastic moduli $G'(\omega)$ and $G''(\omega)$ [57], by using the following expressions which relate $J'(\omega)$ to $G'(\omega)$ and $J''(\omega)$ to $G''(\omega)$

$$J'(\omega) = \frac{1/G'(\omega)}{1 + \tan^2 \delta} \tag{A.10}$$

$$J''(\omega) = \frac{1/G''(\omega)}{1 + (\tan^2 \delta)^{-1}}, \tag{A.11}$$

where δ is the phase difference between the stress and strain. When the equations above are combined with the expressions for $J'(\omega)$ and $J''(\omega)$ from Eq. A.9, we obtain the following expressions:

$$G'(\omega) = \frac{GC^2 + Gk^2\omega^2 + G^2C}{G^2 + C^2 + 2GC + k^2\omega^2} = G\frac{(1 + G/C) + (k\omega/C)^2}{(1 + G/C)^2 + (k\omega/C)^2} \ , \tag{A.12}$$

$$G''(\omega) = \frac{G^2 k\omega}{C^2 + k^2\omega^2 + 2GC + G^2} = G\frac{(G/C)(k\omega/C)}{(1 + G/C)^2 + (k\omega/C)^2} \ . \tag{A.13}$$

Appendix B. Derivation of the 3D frame-invariant form of KH model

Appendix B.1. Relating the stretching tensor to the plastic stretching tensor

One can obtain a simplified relation between the stretching tensor $\mathbf{D} = \frac{1}{2}(\mathbf{L}+\mathbf{L}^\intercal)$ and the plastic stretching tensor $\mathbf{D}^p$ associated with irreversible plastic deformations in the material. To obtain such an expression, the assumption of small elastic deformations must hold. From such an assumption, it follows that the elastic stretch tensor is very close to the identity tensor, i.e. $\mathbf{U}^e \simeq \mathbf{1}$, and therefore from the right polar decomposition of the elastic part of the deformation gradient, $\mathbf{F}^e \simeq \mathbf{R}^e$.

The first step towards obtaining this relation is to write the overall observed velocity gradient $\mathbf{L}$ in terms of the plastic velocity gradient $\mathbf{L}^p$ and the elastic velocity gradient $\mathbf{L}^e$ [5]

$$\mathbf{L} = \mathbf{L}^e + \mathbf{F}^e\mathbf{L}^p\mathbf{F}^{e^{-1}} \ . \tag{B.1}$$

We then show that the stretching tensor $\mathbf{D}$ is equal to the second term on the right hand side in Eq. B.1. By combining Eq. B.1 with the expression $\mathbf{D} = \frac{1}{2}(\mathbf{L} + \mathbf{L}^\intercal)$, the following is obtained:

$$\mathbf{D} = \frac{1}{2}(\mathbf{L} + \mathbf{L}^\intercal) = \frac{1}{2}((\mathbf{L}^e + \mathbf{F}^e\mathbf{L}^p\mathbf{F}^{e^{-1}}) + (\mathbf{L}^e + \mathbf{F}^e\mathbf{L}^p\mathbf{F}^{e^{-1}})^\intercal) \ . \tag{B.2}$$

For Eq. B.2, we first show that $\mathbf{L}^e + \mathbf{L}^{e\intercal} = 0$. We note that:

$$\mathbf{L}^e = \dot{\mathbf{F}}^e\mathbf{F}^{e^{-1}} = (\dot{\mathbf{R}}^e\mathbf{U}^e + \mathbf{R}^e\dot{\mathbf{U}}^e)\mathbf{U}^{e^{-1}}\mathbf{R}^{e^{-1}} = \dot{\mathbf{R}}^e\mathbf{R}^{e^{-1}} \ . \tag{B.3}$$

This follows from $\mathbf{U}^e \simeq \mathbf{1}$ for all times, so the rate of change of elastic stretch $\dot{\mathbf{U}}^e$ is zero. Eq. B.3 implies that $\mathbf{L}^e$ is skew symmetric [5], so its transpose is its negative. Thus $\mathbf{L}^e + \mathbf{L}^{e\intercal} = 0$, so two of the terms in Eq. B.2 cancel out. We now show that the remaining two terms simplify to the second term in Eq. B.1.

$$\mathbf{D} = \frac{1}{2}((\mathbf{F}^e\mathbf{L}^p\mathbf{F}^{e^{-1}}) + (\mathbf{F}^e\mathbf{L}^p\mathbf{F}^{e^{-1}})^\intercal) = \mathbf{R}^e\mathbf{L}^p\mathbf{R}^{e^{-1}} \ , \tag{B.4}$$

where the last equality follows from taking the transpose of the second term, noting that $\mathbf{F}^e \simeq \mathbf{R}^e$, and also noting that $\mathbf{L}^p = \mathbf{D}^p$ (i.e. there is no plastic spin and $\mathbf{L}^p$ is symmetric

- this assumption is justified in [5]). We are left with the following simple equation, which relates $\mathbf{D}$ to $\mathbf{D}^p$:

$$\mathbf{D} = \mathbf{R}^e \mathbf{D}^p \mathbf{R}^{e^{-1}} \ . \tag{B.5}$$

The expression in Eq. B.5 can be used to obtain a functional relationship of the form $\mathbf{T} = f(\mathbf{D})$ in the observed space of the material. We combine Eq. 36 and Eq. 39 to obtain a tensorial expression for $\mathbf{D}$ in terms of the deviatoric Mandel stress $\mathbf{M}_0^e$ and the parameter $\mathbf{A}$:

$$\mathbf{D} = \mathbf{R}^e (d^p \mathbf{N}^p) \mathbf{R}^{e^{-1}} = \mathbf{R}^e \left(\frac{1}{\sqrt{2}} \left(\frac{|\mathbf{M}_0^e - C \log \mathbf{A}|}{\sqrt{2}k} \right)^{1/m} \frac{\mathbf{M}_0^e - C \log \mathbf{A}}{|\mathbf{M}_0^e - C \log \mathbf{A}|} \right) \mathbf{R}^{e^{-1}} \ . \tag{B.6}$$

The expression above provides $\mathbf{D}$ in terms of the deviatoric Mandel stress $\mathbf{M}_0^e$. Recall from the discussion around Fig. 3 that the Mandel stress is associated with the intermediate structural space of the material. We desire to modify Eq. B.6 above so that it is written in terms of the deviatoric Cauchy stress $\mathbf{T}_0$, which is the true or observed stress in the material that would be measured in a rheological experiment. To do this, we note that:

$$\mathbf{M}_0^e = J \mathbf{R}^{e^{-1}} \mathbf{T_0} \mathbf{R}^e \ , \tag{B.7}$$

where J is the determinant of the deformation gradient $\mathbf{F}$. Eq. B.7 above follows from Eqs. 29 and 30, and the fact that $\mathbf{M}^e$ is an isotropic function of $\mathbf{U}^e$ - see pg. 563 of [5] for a guided proof of this. We further restrict our material to be incompressible, so that $J = 1$. We define a new tensorial variable, $\bar{\mathbf{A}}$, which is an evolving internal tensor field which lies in the space of the deformed body (illustrated in Fig. 3). This tensor $\bar{\mathbf{A}}$ is related to $\mathbf{A}$ (which lies in the structural space of the body) as follows:

$$\mathbf{A} = \mathbf{R}^{e^{-1}} \bar{\mathbf{A}} \mathbf{R}^e \ . \tag{B.8}$$

The above equation, together with Eq. B.7, can be substituted into Eq. B.6, in order to cancel out the $\mathbf{R}^e$ and $\mathbf{R}^{e^{-1}}$ tensors outside the parentheses on the right hand side of Eq. B.6. These steps result in the following expression, which provides the rate of deformation tensor $\mathbf{D}$ in terms of the deviatoric Cauchy stress $\mathbf{T}_0$ and this new internal tensorial parameter $\bar{\mathbf{A}}$.

$$\mathbf{D} = \left(\frac{1}{\sqrt{2}} \left(\frac{|\mathbf{T}_0 - C \log \bar{\mathbf{A}}|}{\sqrt{2}k} \right)^{1/m} \frac{\mathbf{T}_0 - C \log \bar{\mathbf{A}}}{|\mathbf{T}_0 - C \log \bar{\mathbf{A}}|} \right) \ . \tag{B.9}$$

References

[1] D. Bonn, M. M. Denn, L. Berthier, T. Divoux, S. Manneville, Yield stress materials in soft condensed matter, Rev. Mod. Phys. 89 (2017) 035005.

[2] H. A. Barnes, The yield stress–a review of $\pi\alpha\nu\tau\alpha$ $\rho\varepsilon\iota$–everything flows?, Journal of Non-Newtonian Fluid Mechanics 81 (1999) 133 – 178.

[3] J. G. Oldroyd, A rational formulation of the equations of plastic flow for a bingham solid, Mathematical Proceedings of the Cambridge Philosophical Society 43 (1947) 100–105.

[4] J. Goddard, Dissipative materials as models of thixotropy and plasticity, Journal of Non-Newtonian Fluid Mechanics 14 (1984) 141 – 160.

[5] M. Gurtin, E. Fried, L. Anand, The Mechanics and Thermodynamics of Continua, Cambridge, 2010.

[6] R. B. Bird, R. C. Armstrong, O. Hassager, Dynamics of Polymeric Liquids Vol. 1, John Wiley and Sons, second edition, 1987.

[7] R. G. Larson, The Structure and Rheology of Complex Fluids, Oxford University Press, 1999.

[8] G. Lipscomb, M. Denn, Flow of bingham fluids in complex geometries, Journal of Non-Newtonian Fluid Mechanics 14 (1984) 337 – 346.

[9] A. N. Beris, J. A. Tsamopoulos, R. C. Armstrong, R. Brown, Creeping motion of a sphere through a bingham plastic, Journal of Fluid Mechanics 158 (1985) 219–244.

[10] N. J. Balmforth, R. V. Craster, R. Sassi, Shallow viscoplastic flow on an inclined plane, Journal of Fluid Mechanics 470 (2002) 1–29.

[11] B. T. Liu, S. J. Muller, M. M. Denn, Convergence of a regularization method for creeping flow of a bingham material about a rigid sphere, Journal of Non-Newtonian Fluid Mechanics 102 (2002) 179 – 191.

[12] G. Vinay, A. Wachs, I. Frigaard, Start-up transients and efficient computation of isothermal waxy crude oil flows, Journal of Non-Newtonian Fluid Mechanics 143 (2007) 141–156.

[13] G. Ovarlez, Q. Barral, P. Coussot, Three-dimensional jamming and flows of soft glassy materials, Nat Mater 9 (2010) 115–119.

[14] L. Martinie, H. Buggisch, N. Willenbacher, Apparent elongational yield stress of soft matter, Journal of Rheology 57 (2013) 627–646.

[15] N. J. Balmforth, I. A. Frigaard, G. Ovarlez, Yielding to stress: Recent developments in viscoplastic fluid mechanics, Annual Review of Fluid Mechanics 46 (2014) 121–146.

[16] A. S. Yoshimura, R. K. Prud'homme, Response of an elastic bingham fluid to oscillatory shear, Rheologica Acta 26 (1987) 428–436.

[17] D. Doraiswamy, A. N. Mujumdar, I. Tsao, A. N. Beris, S. C. Danforth, A. B. Metzner, The Cox–Merz rule extended: A rheological model for concentrated suspensions and other materials with a yield stress,

Journal of Rheology 35 (1991) 647–685.

[18] P. Marmottant, F. Graner, An elastic, plastic, viscous model for slow shear of a liquid foam, European Physical Journal E 23 (2007).

[19] S. Bénito, C. H. Bruneau, T. Colin, C. Gay, F. Molino, An elasto-visco-plastic model for immortal foams or emulsions, European Physical Journal E 25 (2008).

[20] P. Saramito, A new constitutive equation for elastoviscoplastic fluid flows, Journal of Non-Newtonian Fluid Mechanics 145 (2007) 1 – 14.

[21] P. Saramito, A new elastoviscoplastic model based on the Herschel–Bulkley viscoplastic model, Journal of Non-Newtonian Fluid Mechanics 158 (2009) 154 – 161.

[22] J. M. Piau, Carbopol gels: Elastoviscoplastic and slippery glasses made of individual swollen sponges Meso- and macroscopic properties, constitutive equations and scaling laws, Journal of Non-Newtonian Fluid Mechanics 144 (2007) 1–29.

[23] P. Møller, A. Fall, V. Chikkadi, D. Derks, D. Bonn, An attempt to categorize yield stress fluid behavior, Phil. Trans. R. Soc. A 367 (2009) 5139–5155.

[24] P. C. F. Møller, A. Fall, D. Bonn, Origin of apparent viscosity in yield stress fluids below yielding, EPL (Europhysics Letters) 87 (2009) 38004.

[25] M. Denn, D. Bonn, Issues in the flow of yield-stress liquids, Rheologica Acta 50 (2011) 307–315.

[26] P. Saramito, A. Wachs, Progress in numerical simulation of yield stress fluid flows, Rheologica Acta 56 (2017) 211–230.

[27] R. Glowinski, A. Wachs, On the numerical simulation of viscoplastic fluid flow, Handbook of Numerical Analysis 16 (2011) 483–717.

[28] T. C. Papanastasiou, Flows of materials with yield, Journal of Rheology 31 (1987) 385–404.

[29] M. Dinkgreve, M. M. Denn, D. Bonn, "Everything flows?": elastic effects on startup flows of yield-stress fluids, Rheologica Acta 56 (2017) 189–194.

[30] C. J. Dimitriou, R. H. Ewoldt, G. H. McKinley, Describing and prescribing the constitutive response of yield stress fluids using large amplitude oscillatory shear stress (LAOStress), Journal of Rheology 57 (2013) 1–44.

[31] C. J. Dimitriou, G. H. McKinley, A comprehensive constitutive law for waxy crude oil: a thixotropic yield stress fluid, Soft Matter 10 (2014) 6619–6644.

[32] M. Geri, R. Venkatesan, K. Sambath, G. H. McKinley, Thermokinematic memory and the thixotropic elasto-viscoplasticity of waxy crude oils, Journal of Rheology 61 (2017) 427–454.

[33] P. J. Armstrong, C. O. Frederick, A mathematical representation of the multiaxial Bauschinger effect, Materials at High Temperatures 24 (1966) 1–26.

[34] C. Dimitriou, The rheological complexity of waxy crude oils: Yielding, thixotropy and shear hetero-

geneities, Ph.D. thesis, Massachusetts Institute of Technology, 2013.

[35] P. Lidon, L. Villa, S. Manneville, Power-law creep and residual stresses in a carbopol gel, Rheologica Acta 56 (2017) 307–323.

[36] J. Bauschinger, Über die veränderung der position der elastizitätsgrenze des eisens und stahls durch strecken und quetschen und durch erwärmen und abkühlen und durch oftmals wiederholte beanspruchungen, Mitteilung aus dem Mechanisch-technischen Laboratorium der Königlichen polytechnischen Hoschschule in München 13 (1886) 1–115.

[37] Y. Wei, M. J. Solomon, R. G. Larson, A multimode structural kinetics constitutive equation for the transient rheology of thixotropic elasto-viscoplastic fluids, Journal of Rheology 62 (2018) 321–342.

[38] D. Fraggedakis, Y. Dimakopoulos, J. Tsamopoulos, Yielding the yield stress analysis: A thorough comparison of recently proposed elasto-visco-plastic (EVP) fluid models, Journal of Non-Newtonian Fluid Mechanics 238 (2016) 170 – 188.

[39] R. R. Fernandes, D. E. V. Andrade, A. T. Franco, C. O. R. Negro, The yielding and the linear-to-nonlinear viscoelastic transition of an elastoviscoplastic material, Journal of Rheology 61 (2017) 893–903.

[40] D. Fraggedakis, Y. Dimakopoulos, J. Tsamopoulos, Yielding the yield-stress analysis: a study focused on the effects of elasticity on the settling of a single spherical particle in simple yield-stress fluids, Soft Matter 12 (2016) 5378–5401.

[41] P. Coussot, L. Tocquer, C. Lanos, G. Ovarlez, Macroscopic vs. local rheology of yield stress fluids, Journal of Non-Newtonian Fluid Mechanics 158 (2009) 85–90.

[42] M. Dinkgreve, J. Paredes, M. M. Denn, D. Bonn, On different ways of measuring the yield stress, Journal of Non-Newtonian Fluid Mechanics 238 (2016) 233 – 241.

[43] L. Anand, N. M. Ames, V. Srivastava, S. Chester, A thermo-mechanically coupled theory for large deformations of amorphous polymers. Part I: Formulation, International Journal of Plasticity 25 (2008) 1474–1494.

[44] N. M. Ames, V. Srivastava, S. Chester, L. Anand, A thermo-mechanically coupled theory for large deformations of amorphous polymers. Part II: Applications, International Journal of Plasticity 25 (2009) 1495–1539.

[45] D. L. Henann, L. Anand, A large deformation theory for rate-dependent elastic–plastic materials with combined isotropic and kinematic hardening, International Journal of Plasticity 25 (2009) 1833 – 1878.

[46] E. Kroner, Allgemeine kontinuumstheorie der versetzungen und eigenspannungen, Archive for Rational Mechanics and Analysis 4 (1960) 273–334.

[47] M. Habibi, M. Dinkgreve, J. Paredes, M. Denn, D. Bonn, Normal stress measurement in foams and emulsions in the presence of slip, Journal of Non-Newtonian Fluid Mechanics 238 (2016) 33 – 43.

[48] R. B. Bird, R. C. Armstrong, O. Hassager, Dynamics of Polymeric Liquids Vol. 2, John Wiley and Sons, second edition, 1987.

[49] P. Coussot, A. I. Leonov, J. M. Piau, Rheology of concentrated dispersed systems in a low molecular weight matrix, Journal of Non-Newtonian Fluid Mechanics 46 (1993) 179–217.

[50] D. Quemada, Rheological modelling of complex fluids: IV: Thixotropic and "thixoelastic" behaviour. start-up and stress relaxation, creep tests and hysteresis cycles, The European Physical Journal of Applied Physics 5 (1999) 191–207.

[51] K. Dullaert, J. Mewis, A structural kinetics model for thixotropy, Journal of Non-Newtonian Fluid Mechanics 139 (2006) 21–30.

[52] P. R. de Souza Mendes, R. L. Thompson, A critical overview of elasto-viscoplastic thixotropic modeling, Journal of Non-Newtonian Fluid Mechanics 187–188 (2012) 8–15.

[53] J. Mewis, N. J. Wagner, Thixotropy, Advances in Colloid and Interface Science 147–148 (2009) 214–227.

[54] R. H. Ewoldt, G. H. McKinley, Mapping thixo-elasto-visco-plastic behavior, Rheologica Acta 56 (2017) 195–210.

[55] A. Mujumdar, A. N. Beris, A. B. Metzner, Transient phenomena in thixotropic systems, Journal of Non-Newtonian Fluid Mechanics 102 (2002) 157 – 178.

[56] R. G. Larson, Constitutive equations for thixotropic fluids, Journal of Rheology 59 (2015) 595–611.

[57] F. A. Morrison, Understanding Rheology, Oxford University Press, first edition, 2001.